The Journal of Chemical Physics

Theory of ion aggregation and gelation in super-concentrated electrolytes

Cite as: J. Chem. Phys. **152**, 234506 (2020); https://doi.org/10.1063/5.0006197
Submitted: 28 February 2020 . Accepted: 22 May 2020 . Published Online: 19 June 2020

Michael McEldrew, Zachary A. H. Goodwin, Sheng Bi, Martin Z. Bazant, and Alexei A. Kornyshev

AIP Publishing

The Journal of Chemical Physics ARTICLE scitation.org/journal/jcp

Theory of ion aggregation and gelation in super-concentrated electrolytes

Cite as: J. Chem. Phys. 152, 234506 (2020); doi: 10.1063/5.0006197
Submitted: 28 February 2020 • Accepted: 22 May 2020 •
Published Online: 19 June 2020

Michael McEldrew,[1] Zachary A. H. Goodwin,[2,3,4] Sheng Bi,[5] Martin Z. Bazant,[1,6] and Alexei A. Kornyshev[3,4,7,a)]

AFFILIATIONS

[1]Department of Chemical Engineering, Massachusetts Institute of Technology, Cambridge, Massachusetts 02139, USA
[2]Department of Physics, CDT Theory and Simulation of Materials, Imperial College of London, South Kensington Campus, London SW7 2AZ, United Kingdom
[3]Department of Chemistry, Imperial College of London, Molecular Sciences Research Hub, White City Campus, Wood Lane, London W12 0BZ, United Kingdom
[4]Thomas Young Centre for Theory and Simulation of Materials, Imperial College of London, South Kensington Campus, London SW7 2AZ, United Kingdom
[5]State Key Laboratory of Coal Combustion, School of Energy and Power Engineering, Huazhong University of Science and Technology (HUST), Wuhan, Hubei 430074, China
[6]Department of Mathematics, Massachusetts Institute of Technology, Cambridge, Massachusetts 02139, USA
[7]Institute of Molecular Science and Engineering, Imperial College of London, South Kensington Campus, London SW7 2AZ, United Kingdom

[a)]**Author to whom correspondence should be addressed:** a.kornyshev@imperial.ac.uk

ABSTRACT

In concentrated electrolytes with asymmetric or irregular ions, such as ionic liquids and solvent-in-salt electrolytes, ion association is more complicated than simple ion-pairing. Large branched aggregates can form at significant concentrations at even moderate salt concentrations. When the extent of ion association reaches a certain threshold, a percolating ionic gel network can form spontaneously. Gelation is a phenomenon that is well known in polymer physics, but it is practically unstudied in concentrated electrolytes. However, despite this fact, the ion-pairing description is often applied to these systems for the sake of simplicity. In this work, drawing strongly from established theories in polymer physics, we develop a simple thermodynamic model of reversible ionic aggregation and gelation in concentrated electrolytes accounting for the competition between ion solvation and ion association. Our model describes, with the use of several phenomenological parameters, the populations of ionic clusters of different sizes as a function of salt concentration; it captures the onset of ionic gelation and also the post-gel partitioning of ions into the gel. We discuss the applicability of our model, as well as the implications of its predictions on thermodynamic, transport, and rheological properties.

I. INTRODUCTION

For most dilute electrolytes with high permittivity solvents, it is reasonable to assume that the salt is perfectly dissociated as confirmed by classical experiments.[1] However, for moderately concentrated systems or dilute solutions with low permittivity solvents, incomplete dissociation of ions can be substantial.[2] Bjerrum proposed the concept of ion pairing, which was able to account for some deviations of experimental results from theoretical predictions.[3] In the Bjerrum theory of ion pairing, an ion pair is formed when the separation of oppositely charged ions is smaller than the length scale at which the Coulomb interaction is equivalent to thermal energy (known as the Bjerrum length). Many theoretical studies have focused on extending or modifying Bjerrum's treatment/definition of ions pairs, and we direct the readers to Ref. 4 for an extensive review on the topic. Only a small fraction of studies considered ion

aggregates larger than just simple ion pairs,[5–8] but even those works only apply for moderate concentrations and model only simple ionic clusters.

In super-concentrated electrolytes, such as ionic liquids (ILs) or solvent-in-salt electrolytes (SiSEs), the picture is more complicated. With the recent explosion of interest in this regime for electrochemical applications,[9–25] a complete description of ion aggregation may be necessary for understanding the physicochemical, electrochemical, and thermodynamic properties of these concentrated mixtures. For ILs, it has been useful to introduce the concept of free ions, without fully describing the nature of the associated species.[26,27] These concepts have been applied to ILs to reproduce the temperature dependence of ionic conductivities[28] and differential capacitance,[26] although these simple pictures still cannot fully explain the so-called underscreening paradox in ILs.[27,29–32] In SiSEs there have been a multitude of molecular dynamics[33–39] and experimental[37,40,41] studies detailing complex ion association and hydration, often manifesting in highly asymmetric or even negative[42,43] transference numbers. Although these molecular simulations and experimental studies provide valuable insight, it is often constrained to specific systems and is not readily transferable to new systems.

For super-concentrated electrolytes, it would therefore be beneficial to have a theoretical description of ion aggregates of arbitrary size, but to our knowledge, such a theory has not been reported in the literature. Hence, in this article, we will formulate a thermodynamic model of ionic association beyond a simple description of ion pairing (or even triple and quadruple ions). Ultimately, we want our model to capture a distribution of aggregate sizes and even the formation of arbitrarily large ionic aggregates. In building such a model, we draw inspiration from polymer physics. In the early 1940s, Flory[44,45] and Stockmayer[46,47] derived expressions describing the most likely distribution of polymer molecular weights in a mixture. These expressions only require knowledge of the probability of the polymerization reaction, as well as the *functionalities*, f, of the monomers. Functionalities refer to the number of "bonds" a monomer unit can make to extend the polymer. When $f = 2$, large linear chains can be formed, but when $f > 2$, these aggregates will be branched and increasingly complex. Moreover, when $f > 2$, Flory and Stockmayer were able to show that at a certain extent of reaction, a percolating polymer network will be spontaneously formed in a process referred to as gelation. In the polymer community, this percolating network is referred to as a *gel*, while the remaining finite species in the mixture are referred to as the *sol*. The gelation phenomenon outlined by Flory and Stockmayer turned out to be analogous to the percolation problem on a Bethe lattice.[48]

The theories of Flory and Stockmayer were formulated to describe the largely irreversible covalent bond formation characteristic of condensation polymerization reactions, as opposed to the more reversible physical associations of ions. Starting in the late 1980s, Tanaka pioneered the theory of *thermoreversible* polymer association and gelation.[49–56] In his work, Tanaka modeled the physical association between polymer strands within a thermodynamic framework that is able to capture the distribution of polymeric clusters, as well the presence and breadth of gel networks. Of particular interest to us is the two component case in which Tanaka described a mixture of two types of polymer strands that associate heterogeneously in an alternating fashion.[54] This is quite analogous to ion association in that ions will only associate with counterions. Thus, our theory of ion association and gelation in concentrated ionic systems will build upon that of Tanaka.

This paper is split into two main sections: Sections II and III. Section II is further split into six subsections: First, in Sec. II A, we describe the stoichiometric definitions of our mixture, as well as its free energy of mixing. Then, in Sec. II B, we minimize that free energy, yielding our pre-gel cluster distribution in terms of "bare" species volume fractions. In Sec. II C, we introduce "association probabilities" that allow us to write the pre-gel cluster distributions in terms of experimentally accessible overall species volume fractions. In Sec. II D, we describe the mechanism for gelation and derive the criterion for its onset. In Sec. II E, we derive the post-gel relationships, yielding the post-gel cluster distribution and the gel/sol partitioning. In Sec. II F, we propose a method for incorporating excess electrostatic energy into the model. We end the paper by discussing some of our model's implications on observable thermodynamic, transport, and rheological properties of the electrolyte solution, in particular, those properties affected by the presence of the ionic gel. The theory operates with a set of symbols for variables and parameters. For readers' convenience they are listed in Table I.

II. THEORY

We consider a polydisperse mixture of $\sum_{lmsq} N_{lmsq}$ ionic clusters, each containing l cations, m anions, s solvent molecules associated with cations, q solvent molecules associated with anions (*lmsq* cluster), and (if present) an interpenetrating gel network containing N_+^{gel} cations, N_-^{gel} anions, and N_0^{gel} solvent molecules. We model the cations to have a functionality (defined as the number of associations that the species can make) of f_+ and anions to have a functionality of f_-. This means that a(n) cation (anion) is able to associate with f_+ (f_-) anions (cations) or solvent molecules. We also consider the ability of solvent molecules to coordinate to cations or anions with a functionality of 1. This, in fact, means that we neglect the ability of solvent molecules to bridge ionic clusters through interactions with multiple ions and thereby neglect the formation of any solvent-mediated clustering/gelation. This is obviously a simplification, justified by an assumption that the clusters that are not "glued" by direct ion–counter-ion interactions are more labile and as such can be disregarded in the "first approximation." A typical ion cluster consistent with our description is depicted in Fig. 1.

It is necessary to take a moment to justify our application of polymer physics to model super-concentrated electrolytes. Specifically, the functionalities we have introduced may seem better defined for polymer strands or monomers than for ions. Clearly, ions cannot associate with an arbitrarily large number of counterions or solvent molecules. Rather, there is a maximum number of counter-ions or solvent molecules that ions can contact and associate. In our model, the ion functionalities are defined by this maximum coordination number. Moreover, by fixing the number of association sites on an ion (via the functionality), we may directly model the competition of ion association and ion solvation, as well as the crowding of associating species around a specific ion. In fact, in dense ionic systems, there typically are

TABLE I. List of variables and parameters. A star, ⋆, marks the model's phenomenological parameters. If one wishes to compare against a specific experiment or simulation, these parameters can be fitted or determined from more sophisticated theories. The number of free parameters can also be limited through taking limits of this theory, as outlined in the supplementary material.

N_{lmsq}	Number of *lmsq* clusters	N_i^{gel}	Number of species *i* in gel
f_i	Functionality of species *i* (⋆)	v_i	Volume of species *i*
ξ_i	Scaled volume of species *i*	V	Total volume of the mixture
Ω	Number of lattice sites	c_{lmsq}	Concentration of the cluster
c_i^{gel}	Concentration of species *i* in the gel	c_{tot}	Total concentration of clusters
ϕ_i	Total volume fraction of species *i*	$\phi_{\pm}$	Volume fraction of salt
ϕ_i^{sol}	Volume fraction of species *i* in the sol	ϕ_i^{gel}	Volume fraction of species *i* in the gel
ϕ_{lmsq}	Volume fraction of an *lmsq* cluster	ψ_i	Concentration of association sites
Δ_{lmsq}	Free energy of formation of a rank *lmsq* cluster	Δ_{lmsq}^{comb}	Combinatorial free energy of Formation of a rank *lmsq* cluster
Δ_{lmsq}^{bind}	Binding free energy of Formation of an *lmsq* cluster	Δ_{lmqs}^{conf}	Configurational free energy of Formation of an *lmsq* cluster
Δ_{lmsq}^{el}	Electrostatic free energy of Formation of an lmsq cluster	Δ_i^{gel}	Free energy change of species *i* Associating to the gel
μ_{lmsq}	Chemical potential of cluster	μ_i^{gel}	Chemical potential of *i* in gel
K_{lmsq}	Equilibrium constant	W_{lmsq}	Combinatorial enumeration
Δu_{ij}	Association free energy (⋆)	Z	Coordination number of the lattice (⋆)
S_{lmsq}	Configurational entropy of a cluster	S_{lmsq}	Configurational entropy of a cluster
Λ_{ij}	Association constant between *i* and *j* (⋆)	$\tilde{\Lambda}$	Association ratio (⋆)
p_{ij}	Association probabilities	p_{ij}^{sol}	Association probabilities in sol
ζ	Number of anion–cation associations	Γ	Number of cation–solvent associations
Ξ	Number of anion–solvent associations	α	Branching coefficient
$\tilde{n}_w$	Weight average of ionic aggregation	α_{lm}	Fraction of ions in *lm* clusters
w_i^{sol}	Fraction of species in the sol	w_i^{gel}	Fraction of species in the gel
$\mathscr{K}$	Cluster distribution constant	G_e	Equilibrium shear modulus

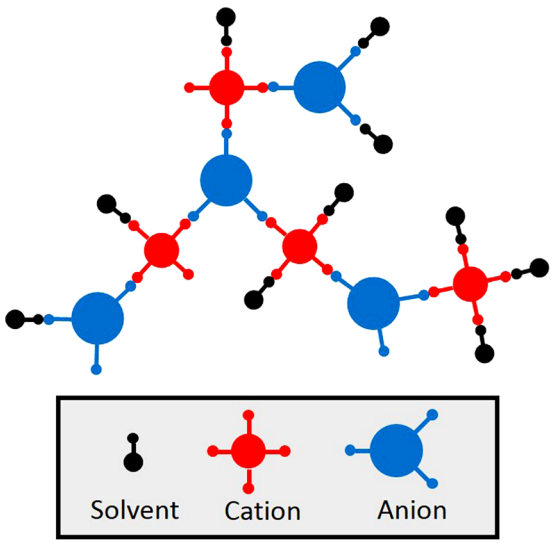

FIG. 1. A cartoon example of cation/anion/solvent clusters that may be found with a certain probability in a model concentrated electrolyte. In this case, we have drawn a cluster in which $f_+ = 4$, $f_- = 3$, $l = 4$, $m = 4$, $s = 7$, and $q = 3$.

preferred configurations for ion associations and functional groups on ions that bridge those associations,[57] quite similar to the polymeric analogs.

Following Tanaka, we account for molecular volumes by using a lattice model. We designate a single lattice site to have the volume of a single solvent molecule, v_0. Thus, the entire volume of the mixture, V, is divided into $\Omega = V/v_0$ lattice sites. Moreover, each cation will occupy $\xi_+ = v_+/v_0$, and an anion will occupy $\xi_- = v_-/v_0$ lattice sites. Furthermore, when a gel is formed, we distinguish between the volume fractions of the gel (superscript *gel*) and sol (superscript *sol*). The volume fractions in the sol and gel constitute the total volume fraction, ϕ_j, of a given species, *j*, which is given by

$$\phi_j = \phi_j^{sol} + \phi_j^{gel}, \tag{1}$$

in which the gel volume fraction is defined as $\phi_j^{gel} = \xi_j N_j^{gel}/\Omega$, with N_j^{gel} as the mole number of species *j* in the gel. The subscript $j = +, -, 0$ corresponds to cation, anion, and solvent, respectively. The sol volume fraction of cations, anions, and solvent molecules, respectively, has the definitions

$$\phi_+^{sol} = \sum_{lmsq} \xi_+ l c_{lmsq}, \tag{2}$$

$$\phi_-^{sol} = \sum_{lmsq} \xi_- m c_{lmsq}, \tag{3}$$

$$\phi_0^{sol} = \sum_{lmsq} (s+q) c_{lmsq}, \tag{4}$$

where $c_{lmsq} = N_{lmsq}/\Omega$ is the dimensionless concentration of an *lmsq* cluster (the number of *lmsq* clusters per lattice site). Similarly, we define $\phi_\pm = \phi_+ + \phi_-$, which is the total volume fraction of the salt in solution. For simplicity, the mixture is assumed to be incompressible, i.e.,

$$1 = \phi_\pm + \phi_0 = \phi_+ + \phi_- + \phi_0. \tag{5}$$

ϕ_+ and ϕ_- are not independent owing to electroneutrality: $\phi_+/\xi_+ = \phi_-/\xi_-$. The reduced volume of the mixture, Ω, can also be expressed in terms of the mole number of each species/component due to the incompressibility constraint [Eq. (5)],

$$\Omega = \sum_{lmsq} (\xi_+ l + \xi_- m + s + q) N_{lmsq} + \xi_+ N_+^{gel} + \xi_- N_-^{gel} + N_0^{gel}. \tag{6}$$

This definition must be used when differentiating the free energy of mixture. Another important quantity that will be used abundantly later in this paper is the dimensionless concentration of association sites (number of association sites per lattice site). We denote this quantity by ψ_j and define it as follows:

$$\psi_j = f_j \phi_j / \xi_j. \tag{7}$$

Thus, ψ_j is the number of j association sites per lattice site. Note that for solvent molecules, $\psi_0 = \phi_0$.

A. Free energy

Thermodynamically, we first treat the electrolyte as an *ideal* mixture of ion/solvent clusters. This means that there will be no inter-cluster interactions (electrostatic or otherwise), although we address later on a potential method for introducing excess electrostatic energy. For now, we neglect the excess electrostatic energy in our model primarily for simplicity, but this neglect fundamentally relies on the assumption that the majority of the electrostatic energy in the mixture is captured via the formation of ion clusters. Implied within the formation of these clusters is that the interactions between species in the clusters are short ranged and constant. Therefore, the association energy between species in a cluster is consistent with a screened electrostatic interaction fixed at a certain distance. Thus, we essentially fix the position at which ions interact, which is not unlike pseudo-lattice-like descriptions of concentrated electrolytes used in the past.[58,59]

Such an approach is different from the classical theories of Bjerrum[3] and more recently in Refs. 60–62. In these works, the authors have taken effort to describe the electrostatic interaction energy required to form an ion association in an ionic atmosphere and an effective dielectric environment. Our work is more concerned with the ability of electrolytes to form more complicated ion clusters undoubtedly present in super-concentrated mixtures. In fact, strong spin-glass, anti-ferromagnetic ordering has been observed in molecular simulations of super-concentrated electrolytes.[63] This ordering is characterized by inherently discrete, many-body short-range correlations, which cannot be captured by theories focusing only on pairwise interactions in an effective medium. By permitting the formation of high order and potentially percolating ionic clusters, we capture some of these strong many-body, short-range correlations observed in Ref. 63. Thus, we eschew the precise microscopic picture of ion association of Refs. 60–62 in favor of a more phenomenological description, which allows us to undertake the additional complexity of high order ionic clustering.

In describing the thermodynamics of an ideal mixture of non-interacting clusters, we employ a Flory-like free energy of mixing given in units of thermal energy, $\beta = 1/k_B T$,

$$\beta \Delta F = \sum_{lmsq} \left[N_{lmsq} \ln(\phi_{lmsq}) + N_{lmsq} \Delta^\theta_{lmsq} \right] + \Delta^{gel}_+(\phi_\pm) N^{gel}_+ + \Delta^{gel}_-(\phi_\pm) N^{gel}_- + \Delta^{gel}_0(\phi_\pm) N^{gel}_0, \tag{8}$$

where $\phi_{lmsq} = (\xi_+ l + \xi_- m + s + q) N_{lmsq}/\Omega$ is the volume fraction of an *lmsq* cluster, Δ^θ_{lmsq} is the free energy of formation of an *lmsq* cluster from its unassociated constituents, and Δ^{gel}_i is the free energy change of species, i, associated with the gel.[49,64,65] Note that we have written Δ^{gel}_i as a function of $\phi_\pm$ for thermodynamic consistency, as we will see later.

The free energy in Eq. (8) contains two essential pieces of physics: the entropy of mixing for a distribution of ion/solvent clusters and the gel, and the association free energy changes corresponding to the formation of clusters or association with the gel. The entropy of mixing takes into account that species within specific clusters are not entropically independent; however, the individual clusters are treated ideally. Additionally, ϕ_{lmsq} is constrained via the incompressibility condition [Eqs. (5) and (6)]. The free energy of mixing in Eq. (8) is written with respect to the reference solutions of pure bare cations, pure bare anions, and pure bare solvent molecules. All species are unassociated in their respective reference states. Additionally, the reference states of pure anions and pure cations are fictitious in that they behave enthalpically as ions in an infinitely dilute electrolyte solution. Thus, the standard state chemical potentials, μ^θ_i, of the ions are that of ions in an infinitely dilute electrolyte. Formally, the free energy of cluster formation is the standard state chemical potential of the cluster subtracted by the standard state chemical potentials of all its bare constituents, $\Delta_{lmsq} = \mu^\theta_{lmsq} - l\mu^\theta_+ - m\mu^\theta_- - (s+q)\mu^\theta_0$.

Differentiating the free energy with respect to N_{lmsq} yields the chemical potential of a cluster rank *lmsq*,

$$\beta \mu_{lmsq} = \ln \phi_{lmsq} + 1 - (\xi_+ l + \xi_- m + s + q) c_{tot} + \Delta^\theta_{lmsq} + d[\phi_0(\xi_+ l + \xi_- m + s + q) - s - q], \tag{9}$$

where $c_{tot} = \sum_{lmsq} c_{lmsq}$ is the total dimensionless concentration (per lattice site), $d = \Delta^{gel\prime}_+ c^{gel}_+ + \Delta^{gel\prime}_- c^{gel}_- + \Delta^{gel\prime}_0 c^{gel}_0$ (the $\prime$ notation refers to a derivative with respect to $\phi_\pm$), and $c^{gel}_i = N^{gel}_i/\Omega$ is the dimensionless concentration of i in the gel (number of species i in the gel per lattice site). Note that we have used the explicit definition of Ω in Eq. (6) when differentiating the free energy.

Additionally, we may define the chemical potential of species immersed in the gel,

$$\beta\mu_{+}^{gel} = \Delta_{+}^{gel} - \xi_{+}c_{tot} + \xi_{+}d\phi_0, \tag{10}$$

$$\beta\mu_{-}^{gel} = \Delta_{-}^{gel} - \xi_{-}c_{tot} + \xi_{-}d\phi_0, \tag{11}$$

$$\beta\mu_{0}^{gel} = \Delta_{0}^{gel} - c_{tot} + d\phi_{\pm}. \tag{12}$$

Establishing an equilibrium between bare species in the sol and species in the gel results in the following expressions for Δ_i^{gel}:

$$\Delta_{+}^{gel}(\phi_{\pm}) = \ln(\phi_{1000}) + 1, \tag{13}$$

$$\Delta_{-}^{gel}(\phi_{\pm}) = \ln(\phi_{0100}) + 1, \tag{14}$$

$$\Delta_{0}^{gel}(\phi_{\pm}) = \ln(\phi_{0010}) + 1, \tag{15}$$

where the bare species' volume fractions (ϕ_{1000}, ϕ_{0100}, ϕ_{0010}) must be solved for in terms of $\phi_{\pm}$ as we will outline in Sec. II C. Thus, Eqs. (13)–(15) demonstrate that Δ_i^{gel} must be a function of $\phi_{\pm}$ for thermodynamic consistency, as mentioned earlier.

B. Pre-gel cluster distribution

The distribution of clusters can be derived by enforcing a chemical equilibrium between all of the clusters and their bare constituents (unassociated components),

$$l[\text{bare cation}]+m[\text{bare anion}]+(s+q)[\text{bare solvent}] \rightleftharpoons [lmsq\ \text{cluster}]. \tag{16}$$

The chemical equilibrium requires that the chemical potentials of bare species and those in clusters are equivalent,

$$l\mu_{1000}+m\mu_{0100}+(s+q)\mu_{0010} = \mu_{lmsq} = l\mu_{lmsq}^{+}+m\mu_{lmsq}^{-}+(s+q)\mu_{lmsq}^{0}. \tag{17}$$

We would like to take a moment to discuss the nature of bare ions with the corresponding chemical potentials μ_{1000} for bare cations and μ_{0100} for bare anions. In dilute electrolytes with typical inorganic salts, the probability of bare ions existing in solution will be nearly negligible; in order to dissolve the salt, the ions must be extensively hydrated. Our use of bare ions in the equilibrium condition [Eq. (17)] does not mean that there will be a significant fraction of bare ions in the electrolyte. Rather, the bare ions (as well as the bare solvent) are used in the equilibrium condition because the bare species are the fundamental "units" that comprise any general cluster. In fact, as we will show, when a good solvent is used, there will be an insignificant fraction of bare ions in solution, in the dilute salt limit, as we would expect from intuition.

Furthermore, note that we may refer to bare solvent molecules with either the index 0001 or 0010. For simplicity, we will use the index 0010 to refer to bare solvent molecules, for the remainder of the text. In Eq. (17), we have defined the chemical potential of a cation, anion, or solvent molecule in an arbitrary cluster in the following manner:

$$\mu_{lmsq}^{+} = \frac{\partial\mu_{lmsq}}{\partial l} = \mu_{1000}, \tag{18}$$

$$\mu_{lmsq}^{-} = \frac{\partial\mu_{lmsq}}{\partial m} = \mu_{0100}, \tag{19}$$

$$\mu_{lmsq}^{0} = \frac{\partial\mu_{lmsq}}{\partial s} = \frac{\partial\mu_{lmsq}}{\partial q} = \mu_{0010}. \tag{20}$$

Solving Eq. (17) for an arbitrary $lmsq$ cluster obtains the following relation:

$$\phi_{lmsq} = K_{lmsq}\phi_{1000}^{l}\phi_{0100}^{m}\phi_{0010}^{s+q}, \tag{21}$$

where ϕ_{1000}, ϕ_{0100}, and ϕ_{0010} are the bare species' volume fractions of cations, anions, and solvent molecules, respectively, and K_{lmsq} is the equilibrium constant, given by

$$K_{lmsq} = \exp(l + m + s + q - 1 - \Delta_{lmsq}^{\theta}). \tag{22}$$

Thus, the partitioning of the species into clusters of different sizes is strongly governed by Δ_{lmsq}^{θ}. As such, this is where much of the physics of the ion/solvent association will be included. It contains three contributions,

$$\Delta_{lmsq}^{\theta} = \Delta_{lmsq}^{comb} + \Delta_{lmsq}^{bind} + \Delta_{lmsq}^{conf}, \tag{23}$$

where Δ_{lmsq}^{comb} is the *combinatorial* (entropic) contribution, describing the multiplicity of clusters with the same number of constituents; Δ_{lmsq}^{bind} is the *binding* contribution, describing the binding energy of the constituents in the cluster; and Δ_{lmsq}^{conf} is the *configurational* contribution, describing the configurational entropy change upon forming a cluster from base constituents. We would like to emphasize that the binding contribution is largely electrostatic in nature. As we have previously mentioned, the fact that we have neglected electrostatic interactions between clusters relies on the assumption that the majority of the electrostatic energy is incorporated in the formation of the ion clusters (via this binding contribution), as opposed to between different clusters.

The entropy associated with the combinatorial enumeration, W_{lmsq}, of all of the possible ways a cluster with l cations, m anions, and $s + q$ solvent molecules can be formed is given by

$$\Delta_{lmsq}^{comb} = -\ln\left(W_{lmsq}\right). \tag{24}$$

To derive W_{lmsq}, we use a two step procedure. First, we enumerate the number of ways to construct a network containing l anions and m cations, which are associated together in an alternating fashion, W_{lm}. This combinatorial problem is well known,[66]

$$W_{lm} = \frac{(f_{+}l - l)!(f_{-}m - m)!}{l!m!(f_{+}l - l - m + 1)!(f_{-}m - l - m + 1)!}. \tag{25}$$

In the second step, we enumerate the number of ways $s + q$ solvent molecules can be placed on the cation–anion cluster. We know that we may only place the s solvent molecules on the remaining $f_{+}l - l - m + 1$ open cation sites. Thus, s must be less than or equal to $f_{+}l - l - m + 1$. This enumeration is expressed via the binomial coefficient

$$\mathscr{C}_{s}^{f_{+}l-l-m+1} = \frac{(f_{+}l - l - m + 1)!}{s!(f_{+}l - l - m - s + 1)!}. \tag{26}$$

Similarly, we must place q solvent molecules on the remaining $f_{-}m - m - l + 1$ open anion sites, which can be enumerated via

$$\mathscr{C}_{q}^{f_{-}m-m-l+1} = \frac{(f_{-}m - m - l + 1)!}{q!(f_{-}m - m - l - q + 1)!}. \tag{27}$$

Thus, we have

$$W_{lmsq} = W_{lm}\mathscr{C}_s^{f_+l-l-m+1}\mathscr{C}_q^{f_-m-m-l+1} = \frac{(f_+l-l)!(f_-m-m)!}{l!m!s!q!(f_+l-l-m-s+1)!(f_-m-m-l-q+1)!}. \quad (28)$$

Next, the binding contribution, Δ_{lmsq}^{bind}, is described simply via the binding free energies: Δu_{ij} between species i and j, where $i \neq j$ and $\Delta u_{ij} = \Delta u_{ji}$. As we have mentioned, these binding energies, especially the ionic association energy, are largely electrostatic in nature. Here, we assume that the association energy is a simple constant, which would be consistent with a screened electrostatic interaction at a fixed distance.

Recall that our model does not allow for solvent molecules to form clusters among themselves. For this reason, if a cluster contains 0 cations and anions, the cluster will necessarily only contain a single solvent molecule, corresponding to a bare solvent molecule. Thus, $\Delta_{0010}^{bind} = \Delta_{0001}^{bind} = 0$. Overall, we can write Δ_{lmsq}^{bind} as

$$\Delta_{lmsq}^{bind} = [(l+m-1)\Delta u_{+-} + s\Delta u_{+0} + q\Delta u_{-0}] \times [1 - \delta_{l,0}\delta_{m,0}(\delta_{q,0}\delta_{s,1} + \delta_{q,1}\delta_{s,0})], \quad (29)$$

where $\delta_{i,j}$ is the Kronecker delta function. For $l + m > 0$, the association free energy for an $lmsq$ cluster is

$$\Delta_{lmsq}^{bind} = (l+m-1)\Delta u_{+-} + s\Delta u_{+0} + q\Delta u_{-0}. \quad (30)$$

The coefficient in front of the cation–anion binding energy, Δu_{+-}, is due to the fact that there must be many cation–anion associations to form a cluster with l cations and m anions.

For the configurational contribution, Δ_{lmsq}^{conf}, we use Flory's lattice theoretical expression for the entropy of disorientation.[64,65] Tanaka adapted and modified Flory's expression for more complicated associating polymer mixtures in Refs. 49, 55, and 67, through a procedure outlined by Flory, involving the subsequent placement of lattice sized bits of molecules onto adjacent lattice sites. From this, we write the configurational entropy, S_{lmsq}, of an $lmsq$ cluster as

$$S_{lmsq} = -\ln\left(\frac{(\xi_+l + \xi_-m + s + q)Z(Z-1)^{\xi_+l+\xi_-m+s+q-2}}{\exp(\xi_+l + \xi_-m + s + q - 1)}\right), \quad (31)$$

where Z is the coordination number of the lattice. The configurational bit of Δ_{lmsq} is then

$$\Delta_{lmsq}^{conf} = S_{lmsq} - lS_{1000} - mS_{0100} - (s+q)S_{0010} = -\ln\left(\frac{(\xi_+l + \xi_-m + s + q)\left[(Z-1)^2/Ze\right]^{l+m+s+q-1}}{\xi_+^l\xi_-^m}\right). \quad (32)$$

Having defined each component of Δ_{lmsq}^{θ}, it is useful to introduce the notion of the "association constant," Λ_{ij}, for the association of species i and j. The association constant characterizes the driving force or affinity—or more accurately, the exponentiated driving force/affinity—for a specific type of association. It is written as follows:

$$\Lambda_{+-} = \frac{(Z-1)^2}{Z}\exp(-\Delta u_{+-}). \quad (33)$$

The ion–solvent association constant, $\Lambda_{\pm 0}$, contains only a non-electrostatic part of the association constant,

$$\Lambda_{\pm 0} = \frac{(Z-1)^2}{Z}\exp(-\Delta u_{\pm 0}). \quad (34)$$

We then plug in each contribution of Δ_{lmsq}^{θ} into Eq. (21). Due to the Kronecker deltas in Eq. (29), the distribution is most easily written separately for clusters containing ions and bare solvent molecules. First, for ion-containing clusters ($l + m \geq 1$), we obtain the distribution

$$c_{lmsq} = \frac{W_{lmsq}}{\Lambda_{+-}}(\psi_{1000}\Lambda_{+-})^l(\psi_{0100}\Lambda_{+-})^m \times (\phi_{0010}\Lambda_{+0})^s(\phi_{0010}\Lambda_{-0})^q, \quad (35)$$

where $\psi_{1000} = f_+\phi_{1000}/\xi_+$ and $\psi_{0100} = f_+\phi_{0100}/\xi_+$ are the number of association sites per lattice site for bare cations and bare anions, respectively. For clusters not containing ions, the only non-zero component of the distribution corresponds to bare solvent molecules,

$$c_{0010} = c_{0001} = \phi_{0010}. \quad (36)$$

Equations (35) and (36) give the thermodynamically consistent number distribution for clusters in the electrolyte mixture. It can readily give the volume fraction of a cluster of any size and makeup, if the volume fraction of the bare cations, anions, and solvent molecules is known. However, these bare species volume fractions are not experimentally accessible. Thus, we must write the volume fractions of the bare species in terms of the overall salt/solvent fractions, which are experimentally accessible.

C. Association probabilities

Once again, we follow Tanaka by introducing the association probabilities, p_{ij}. These probabilities are useful because we may write the bare species' volume fractions in terms of them. Formally, p_{ij} is defined as the fraction of association sites of species, i, that are occupied in association with species, j. Recall that cations, anions, and solvent molecules are said to have f_+, f_-, and 1 association site per molecule, respectively. This implies that generally $p_{ij} \neq p_{ji}$, unless the functionalities and concentrations of species i and j are equivalent, as we will show below. We may write, assuming independent associations, the bare cation volume fraction as

$$\phi_{1000} = \phi_+(1 - p_{+-} - p_{+0})^{f_+}. \quad (37)$$

The above equation arises because the probability that a given cation association site will be "dangling" (not participating in associations) will be $1 - p_{+-} - p_{+0}$. Thus, the probability for all f_+ sites to be dangling is $(1-p_{+-}-p_{+0})^{f_+}$. Analogously, for the bare anions and solvent molecules, we have

$$\phi_{0100} = \phi_-(1 - p_{-+} - p_{-0})^{f_-}, \quad (38)$$

$$\phi_{0010} = \phi_0(1 - p_{0+} - p_{0-}). \quad (39)$$

We may insert Eqs. (37)–(39) into Eq. (35), obtaining a cluster distribution in terms of overall species volume fractions and the association probabilities, p_{ij}. However, we now have six new variables, p_{ij}, which are unknown and a function of the overall species volume fractions. Thus, we need six equations to determine these

six unknowns. We can obtain three equations straight away due to a conservation of each type of association. For cation–anion associations, we have

$$\psi_+ p_{+-} = \psi_- p_{-+} = \zeta, \tag{40}$$

where ζ is the number of cation–anion associations per lattice site. For cation–solvent associations, we have

$$\psi_+ p_{+0} = \phi_0 p_{0+} = \Gamma, \tag{41}$$

where Γ is the number of cation–solvent associations per lattice site. Finally, for anion–solvent associations, we have

$$\psi_- p_{-0} = \phi_0 p_{0-} = \Xi, \tag{42}$$

where Ξ is the number of anion–solvent associations per lattice site.

We obtain the last three equations following Tanaka, by employing the law of mass action on the number of associations using the association constants Λ_{+-}, Λ_{+0}, and Λ_{+0}. For cation–anion associations, we have

$$\Lambda_{+-}\zeta = \frac{p_{+-}p_{-+}}{(1-p_{+-}-p_{+0})(1-p_{-+}-p_{-0})}. \tag{43}$$

Similarly, for the cation–solvent associations, we have

$$\Lambda_{+0}\Gamma = \frac{p_{+0}p_{0+}}{(1-p_{+-}-p_{+0})(1-p_{0+}-p_{0-})}. \tag{44}$$

Finally, for the anion–solvent associations, we have

$$\Lambda_{-0}\Xi = \frac{p_{-0}p_{0-}}{(1-p_{-+}-p_{-0})(1-p_{0+}-p_{0-})}. \tag{45}$$

Here, Λ_{+-}, Λ_{+0}, and Λ_{-0} are treated as equilibrium constants for the individual associations made. Similar mass action laws have been used in the past to treat ion pair formation,[3,60–62] in which the association constants were determined self-consistently from the interaction potential between the associating species. This type of procedure would be complicated by the formation of complex ion/solvent aggregates and is beyond the scope of our current work.

Thus, Eqs. (40)–(45) provide six equations from which we may find each p_{ij} in terms of the overall species volume fractions. Without making approximations, we cannot obtain an analytical solution to this system of equations, but nonetheless, we may solve it numerically. A useful approximation based on assumptions of ion symmetry and "stickiness" permits an analytical solution of the association probabilities in terms of overall species volume fractions and is outlined in the supplementary material. These association probabilities close the model so that we may now obtain the full distributions of clusters as a function of the overall electrolyte composition.

In Fig. 2, we plot sample curves of the concentration dependence of these association probabilities. The parameters detailed in the caption of Fig. 2, which will be used for the majority of this paper, were chosen to be representative of salts used in typical water-in-salt electrolytes (WiSEs), such as lithium bis(trifluoromethanesulfonyl) imide (LiTFSI),[11] sodium trifluoromethane sulfonate (NaOTF),[17] or even potassium containing analogs.[23] Note that although these salts have extremely high solubility limits, they would likely precipitate from solution prior to reaching the pure salt limit ($x = 1$). Nevertheless, our figures will extend to the pure salt limit, in order to explore the behavior of the model in this regime. Furthermore, for different sets of parameters that are more representative of an ionic liquid salt, for example, the pure salt limit would be extremely relevant.

Thus, the parameters used in most of our examples represent a model water-in-salt electrolyte. As would be expected for a LiTFSI-water or NaOTF-water system, the cation–solvent association constant ($\Lambda_{+0} = 500$) is considerably larger than the anion–solvent

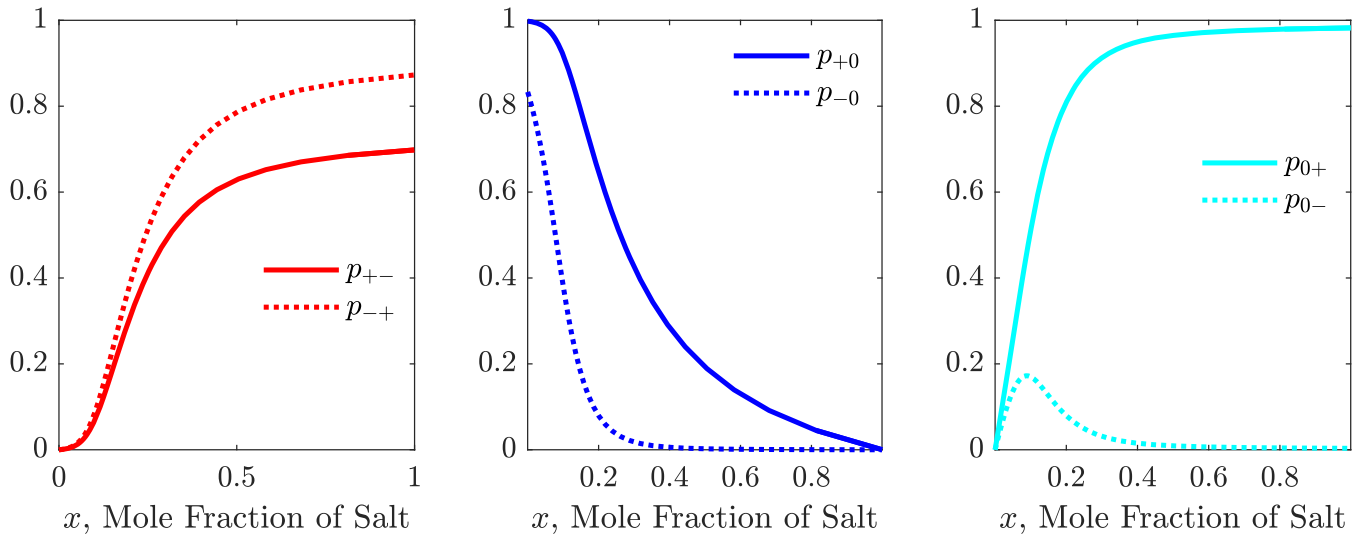

FIG. 2. Association probabilities, p_{ij}, as a function of the mole fraction of salt for a model water-in-salt electrolyte. The ion–counter-ion association probabilities are plotted in the left panel (p_{+-} and p_{-+}), the ion–solvent association probabilities are plotted in the middle panel (p_{+0} and p_{-0}), and the solvent–ion associations are plotted in the right panel (p_{0-} and p_{0+}). These curves are generated for $\xi_+ = 1$, $\xi_- = 10$, $\Lambda_{+-} = 50$, $\Lambda_{+0} = 500$, $\lambda_{-0} = 5$, $f_+ = 5$, $f_- = 4$.

association constant ($\lambda_{-0} = 5$). The anion is also made to be much larger ($\xi_- = 10$) than the cation ($\xi_+ = 1$). Additionally, the cation has a larger functionality $f_+ = 5$ than the anion ($f_- = 4$) to emphasize further cation/anion asymmetry.

The ion–counter-ion association probabilities, $p_{\pm\mp}$ (left panel in Fig. 2), increase monotonically with salt volume fraction, and the difference between the solid and dotted blue curves in Fig. 2 comes from the difference in cation and anion functionality; for a given total number of cation–anion associations, a lower fraction of cation association sites will be occupied with associations with anions.

The ion–solvent association probabilities, $p_{\pm 0}$ (middle panel in Fig. 2), both decrease monotonically with the increase in ion concentration. This monotonically decreasing behavior is expected because there is less water available to associate to ions, and more associations with counter-ions at high salt volume fractions. Again, the solvent is more likely to associate with cations because the association constants considered here dictate the solvent to interact stronger with cations than anions. In the dilute limit, the ion–solvent association probability tends toward $\lambda_{\pm 0}/(\lambda_{\pm 0} + 1)$. Thus, for the vigorously solvated cation, only an extremely small fraction (0.2%) of cation association sites are not occupied with an association with solvent molecules in the dilute limit. This would correspond to a fraction of bare cations (not associated with anything) of 3.2×10^{-12}%, which is consistent with our aforementioned assertion that for vigorously solvated ions, the fraction of bare ions will be negligible.

The cation:anion asymmetry in functionality is manifested most clearly for the solvent–ion association probabilities, $p_{0\pm}$ (right panel in Fig. 2). The solvent–cation association probability increases monotonically with the salt volume fraction due to the increase in the concentration of cations and thus cationic association sites. However, the same argument does not hold for the solvent–anion association probability, which displays non-monotonic behavior. Initially, p_{0-} increases due to the increase in anion concentration but then decreases because the cations monopolize the solvent association at high ion concentrations. The reason for this is that our chosen parameters dictate that cations associate more favorably than anions with solvent molecules. ($\Lambda_{+0} > \Lambda_{-0}$). Moreover, cations also have more association sites than anions ($f_+ > f_-$) and thus can accept more solvent associations.

D. Sol/gel transition

Since the functionalities, $f_\pm$, of anions and cations are both greater than two, the clusters have the potential to become infinitely large if the probabilities, p_{+-} and p_{-+}, are large enough. The point at which this occurs (i.e., the gelation point) can be determined in the following manner with the help of Fig. 3. Consider, for example, that we traverse along a specific branch of the cluster until we stop arbitrarily at a cation, labeled "1" in Fig. 3. The cation contains $f_+ - 1$ sites in addition to the site that was traversed to arrive at the cation. In order for the cluster to proceed infinitely—thus forming a gel—one of the additional $f_+ - 1$ sites must continue the chain with a probability of unity,[68]

$$(f_+ - 1)\alpha^* = 1, \tag{46}$$

where α (not to be confused with the fraction of free species, α_+, α_-, or α_0, which will be defined later) is known as the branching coefficient with "$*$" denoting its critical value for gelation, and the

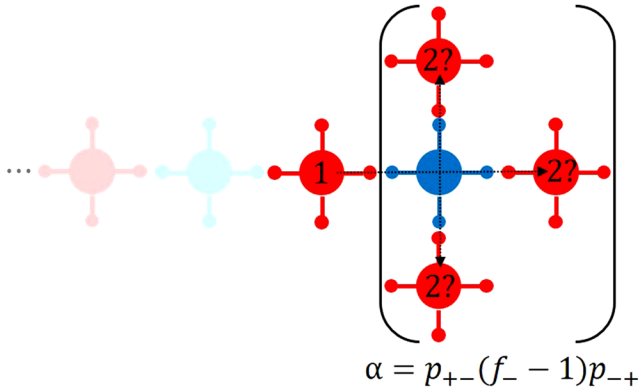

FIG. 3. A schematic illustrating the concept of the branching coefficient, α, which is an essential quantity in determining the criterion for gelation [Eq. (46)]. Starting at the node labeled 1 (referring to a cation), we note that the cluster proceeds arbitrarily to the left. We then consider the probability (α) of the cluster continuing to the right to the next cationic node (marked as 2 with a "?" to denote that the cluster may continue to any one of these cations). In order for the cluster to continue to the right, the cationic node marked 1 must associate with an anion (with probability p_{+-}) and then one of the $f_- - 1$ remaining anionic association sites must associate with another cation (with probability p_{-+}). Thus, the branching coefficient, α is the compounding of the probabilities for a cluster to proceed from cation 1 to an anion and then to any of the cations marked with a 2.

factor of $f_+ - 1$ arises because there are $f_+ - 1$ additional branches on the cation capable of extending the cluster. The same criterion arises for mean-field percolation on a Bethe lattice with a coordination number of f_+.[48] In our case, though, α refers to the probability that cation 1 continues to a subsequent cationic node (labeled 2 in Fig. 3) along any available branch, as depicted by the dotted arrows in Fig. 3. In order to get from one cationic node to the next cationic node, we require that one of the cation sites associates with an anion with probability p_{+-} and that one of the $f_- - 1$ remaining anionic sites reacts with a cation with probability p_{-+}. Thus,

$$\alpha = p_{+-}(f_- - 1)p_{-+}. \tag{47}$$

The criterion for gelation is then

$$(f_+ - 1)p^*_{+-}(f_- - 1)p^*_{-+} = 1. \tag{48}$$

If this criterion is met, then we expect a macroscopic ionic gel network to spontaneously form and percolate through the electrolyte. Thus, if we know the probabilities, p_{+-} and p_{-+}, as functions of concentration, then we may predict the critical concentration at which gelation will occur using Eq. (48).

We can also see this criterion arise when analyzing the weight averaged degree of ionic aggregation, $\bar{n}_w$ (the average sized cluster of which an ion is a part), which is defined by the following formula:

$$\bar{n}_w = \frac{\sum_{lmsq}(l+m)^2 c_{lmsq}}{\sum_{lmsq}(l+m)c_{lmsq}}. \tag{49}$$

We can then plug in Eq. (35) and perform the sum over s and q by invoking the binomial theorem obtaining

$$\bar{n}_w = \sum_{lm}(l+m)\alpha_{lm}, \tag{50}$$

where α_{lm} is the fraction of total ions in clusters containing l cations and m anions. For clusters containing more than one ion, α_{lm} is given by

$$\alpha_{lm} = \frac{\mathscr{K}}{2}(l+m)W_{lm}\left(\frac{p_{-+}}{1-p_{-+}}(1-p_{+-})^{f_+-1}\right)^l \times \left(\frac{p_{+-}}{1-p_{+-}}(1-p_{-+})^{f_--1}\right)^m, \quad (51)$$

where $\mathscr{K} = f_+(1-p_{+-})(1-p_{-+})/p_{-+}$ (analogously defined by Stockmayer in Ref. 66).

We can write the sum in Eq. (50) in a closed form with the help of Stockmayer (Ref. 66) or with the methods developed within Ref. 69,

$$\bar{n}_w = 1 + \frac{p_{+-}p_{-+}((f_+-1)p_{+-}+(f_--1)p_{-+}+2)}{\left(\frac{p_{+-}}{f_-}+\frac{p_{-+}}{f_+}\right)(1-(f_+-1)(f_--1)p_{+-}p_{-+})}. \quad (52)$$

Thus, $\bar{n}_w$ diverges when $(f_+-1)p_{+-}(f_--1)p_{-+} = 1$, which is the exact condition we previously derived for gelation.

As an example, we plot the weight averaged degree of aggregation as a function of concentration in Fig. 4 using Eq. (52) with the model parameters listed in the caption, corresponding to the aforementioned fictitious water-in-salt electrolyte. As can be seen, the weight average degree of aggregation diverges at the gelation point. In the inset of Fig. 4, we display a log–log plot of the weight average degree of aggregation as a function of deviation of the product $p_{+-}p_{-+}$ from the critical value, yielding a linear curve with a slope of −1. Thus, $\bar{n}_w$ diverges at the gel point with a critical exponent of −1. This type of behavior is expected, when considering the direct analogy of our gelation model with percolation on a Bethe lattice.

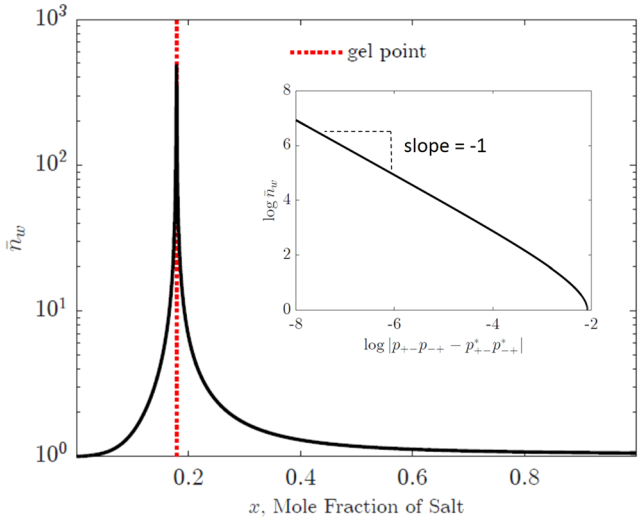

FIG. 4. The weight averaged degree of ion aggregation, $\bar{n}_w$, plotted against the volume fraction of salt, $\phi_\pm$, using Eq. (52) with probabilities for association restricted to the sol (excluding the gel). In the inset, we plot (on a log–log scale) the weight averaged degree of ion aggregation, $\bar{n}_w$, against the deviation from the gel point, $|p_{+-}p_{-+} - p^*_{+-}p^*_{-+}|$, showing a critical exponent of −1. This curve was generated for $\xi_+ = 1$, $\xi_- = 10$, $\Lambda_{+-} = 50$, $\Lambda_{+0} = 500$, $\lambda_{-0} = 5$, $f_+ = 5$, $f_- = 4$.

Interestingly, in Fig. 4, beyond the gel point, $\bar{n}_w$ rapidly decreases. This is because we plot the weight averaged degree of aggregation for species in the sol only, excluding the gel. After the gel forms, the vast majority of ion associations contribute to the gel, as opposed to finite clusters in the sol. As we approach the no-solvent limit (ionic liquid/crystal limit), the degree of aggregation in the sol is essentially 1, implying that at large salt fractions, the electrolyte looks like a simple mixture of dilute free ions immersed in an ionic gel.

E. Post-gel regime

For salt concentrations beyond the critical concentration, we expect a gel to be present in the electrolyte containing an increasing fraction of the electrolyte's ions. Thus, we must quantify the fraction of the species in the gel and in the sol. We employ Flory's treatment of the post-gel regime in which the volume fraction of bare species can be written equivalently in terms of overall association probabilities, p_{ij}, and association probabilities taking into account only the species residing in the sol, p_{ij}^{sol},

$$\phi_+(1-p_{+-}-p_{+0})^{f_+} = \phi_+^{sol}(1-p_{+-}^{sol}-p_{+0}^{sol})^{f_+}, \quad (53)$$

$$\phi_-(1-p_{-+}-p_{-0})^{f_-} = \phi_-^{sol}(1-p_{-+}^{sol}-p_{-0}^{sol})^{f_-}, \quad (54)$$

$$\phi_0(1-p_{0+}-p_{0-}) = \phi_0^{sol}(1-p_{0+}^{sol}-p_{0-}^{sol}), \quad (55)$$

where ϕ_i^{sol} is the volume fraction of species, i remaining in the sol. We may determine each of the three unknown ϕ_i^{sol} variables, as well as the six unknown sol association probabilities, p_{ij}^{sol}, using (53)–(55) in addition to Eqs. (40)–(45); however, in this case, we use sol-specific quantities.

Thus, we have nine equations and nine unknowns (six sol association probabilities and three sol species volume fractions). The fraction of species, i, in the gel is simply given by

$$w_i^{gel} = 1 - \phi_i^{sol}/\phi_i. \quad (56)$$

Note that prior to the critical gel concentration, we have the trivial solution that $p_{ij} = p_{ij}^{sol}$ and $\phi_i = \phi_i^{sol}$, yielding a gel fraction of $w_i^{gel} = 0$. However, beyond the gel point, there is a non-trivial solution yielding $w_i^{gel} > 0$.

As an example, we plot the "sol" association probabilities in Fig. 5 using the model parameters listed in the caption, corresponding to the aforementioned fictitious water-in-salt electrolyte. As expected, we observe distinct cusps in the "sol" association probabilities at the gel point. These cusps are the result of a bifurcation in the solutions to the equations. One solution branch belongs to the overall association probabilities that transition smoothly through the gel point, and the other solution branch belongs to the "sol" association probabilities that bifurcate from the gel point. Generally, beyond the gel point, the sol association probabilities decrease because the majority of associations are consumed by the gel, causing species to be more "free" in the sol. We see this generality break for p_{+0}^{sol} in the middle panel of Fig. 5. Immediately beyond the gel point, p_{+0}^{sol} increases due to the fact that the cation–anion association strongly decreases in the sol. The decreasing ion association in the

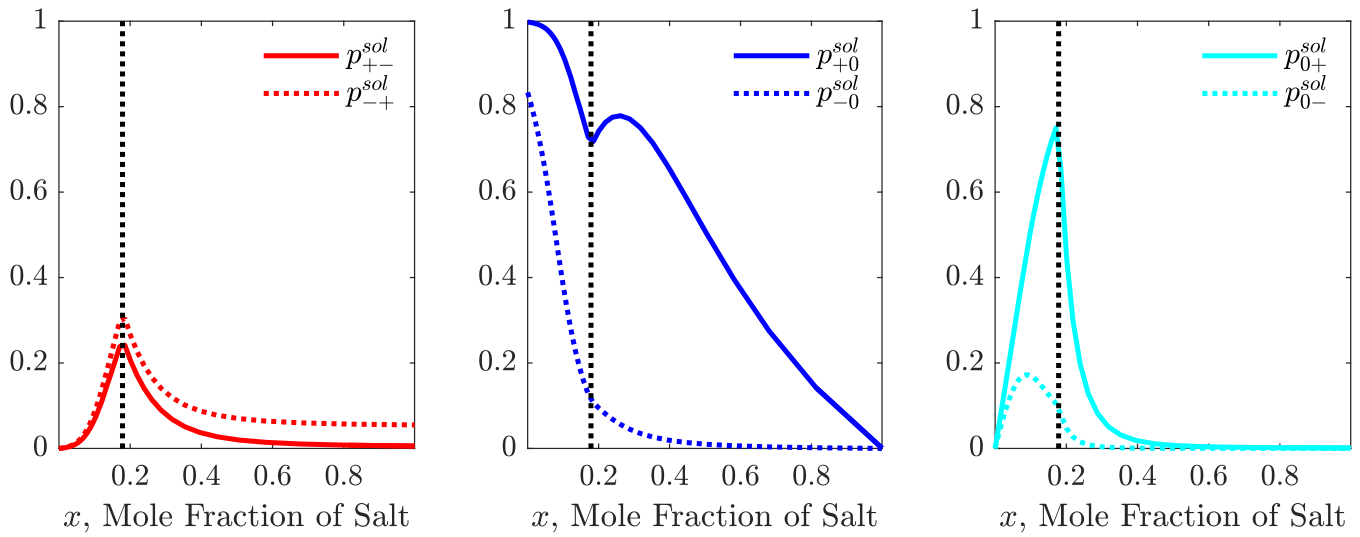

FIG. 5. The "sol" association probabilities, p^{sol}_{ij}, are plotted against the mole fraction of salt. The ion–counter-ion association probabilities (p^{sol}_{+-} and p^{sol}_{-+}) are plotted in the left panel, the ion–solvent association probabilities (p^{sol}_{+0} and p^{sol}_{-0}) are plotted in the middle panel, and the solvent–ion associations (p^{sol}_{0-} and p^{sol}_{0+}) are plotted in the right panel. These curves are generated for $\xi_+ = 1$, $\xi_- = 10$, $\Lambda_{+-} = 50$, $\Lambda_{+0} = 500$, $\lambda_{-0} = 5$, $f_+ = 5$, $f_- = 4$. The vertical black dotted line corresponds to the gel point.

sol means that ions in the sol become slightly more free to associate with solvent, especially the cations ($\lambda_{+0} >> 1$). Eventually, the overall decreasing solvent fraction causes p^{sol}_{+0} to strongly decrease at high salt mole fractions.

In the left panel of Fig. 6, we plot the concentration dependence of various ion clusters of different sizes ($1 \le l + m \le 10$ and the ionic gel). We note that the yellow curve in Fig. 6 corresponds to the fraction of so-called "free ions." Free ions are ions that are simply not associated with counter-ions but can be solvated to any degree. This should not be confused with our naming of bare ions, which are ions not associated with anything. As expected, we see that the fraction of free ions ($l + m = 1$) decreases monotonically as a function of salt volume fraction due to the increase in ionic association probability. Interestingly, all other finite ion clusters behave non-monotonically with salt fraction. In general, ion clusters with $l + m \ge 2$ first increase with salt concentration due to the increase in ion association probability. However, as salt concentration increases further, more and more associations are directed toward the formation of higher order clusters and eventually the ionic gel. Figure 6 also defines three distinct "regimes" in the solution. In the low concentration regime ($0 < \phi_\pm \le 0.15$), free ions are the major ionic species in the electrolyte. For $0.2 < \phi_\pm \le 0.3$, finite ion clusters dominate the electrolyte. Finally, for high salt concentrations ($\phi_\pm > 0.3$), the electrolyte is majorly comprised of the ionic gel.

In the right panel of Fig. 6, we plot the same cluster fractions but consider only the ions that remain in the sol. The curves are identical to those in the left plot of Fig. 6 prior to the gel point. Beyond the gel point, the cluster fractions behave in a very peculiar manner. The

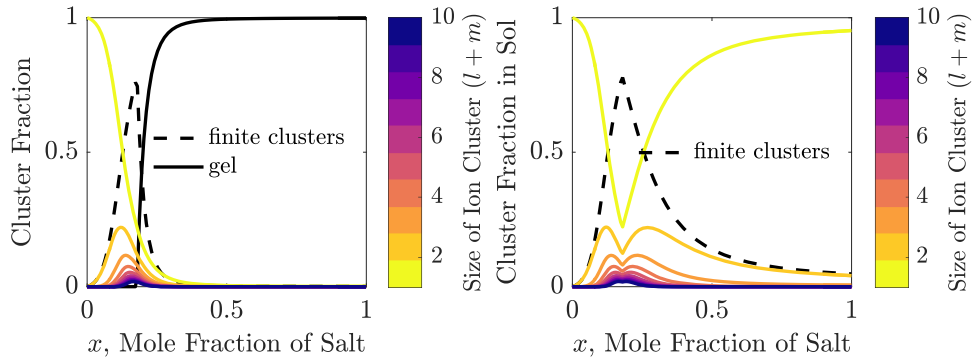

FIG. 6. Fraction of ion clusters of different sizes ($l + m$), including both total finite cluster fraction ($l + m \ge 2$) and the gel fraction as a function of salt volume fraction. Thus, the black dashed curve corresponds to all finite clusters excluding the free ions; free ions are depicted by the yellow curve; and the solid black curve corresponds to the fraction of gel. The plot on the left corresponds to cluster fractions considering all ions in the electrolyte, while the right corresponds to cluster fractions for ions in the sol only. These curves are generated for $\xi_+ = 1$, $\xi_- = 10$, $\Lambda_{+-} = 50$, $\Lambda_{+0} = 500$, $\lambda_{-0} = 5$, $f_+ = 5$, $f_- = 4$.

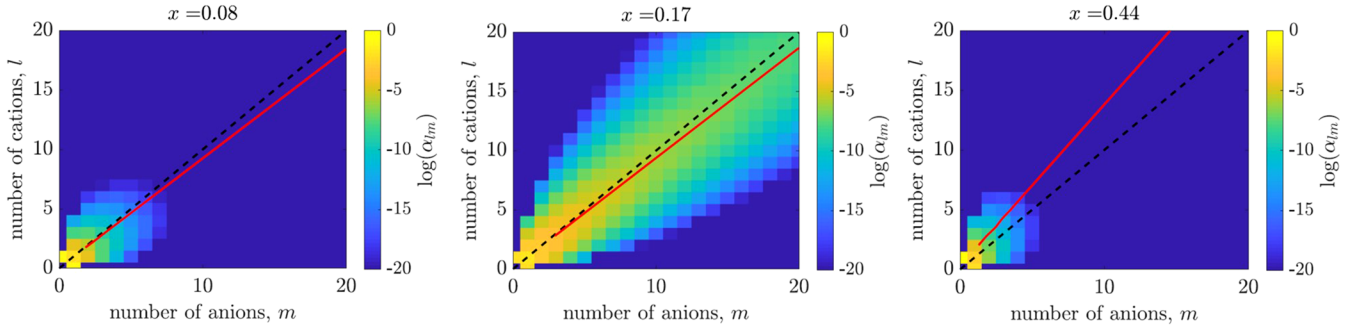

FIG. 7. Probability distribution of ion clusters rank *lm* (containing *l* cations and *m* anions) for various mole fractions of salt. (Left) The cluster distribution for a pre-gel salt mole fraction of $x = 0.08$. (Middle) The cluster distribution for a near-gel salt mole fraction of $x = 0.17$. (Right) The cluster distribution for a post-gel salt mole fraction of $x = 0.44$. In each plot, the black dashed curve corresponds to a 1:1 anion:cation ratio, and the solid red curve corresponds to the most probable cluster of total rank $l + m$. Note that the probabilities are plotted on a log scale to better visualize the distribution. These plots are generated for $\xi_+ = 1$, $\xi_- = 10$, $\Lambda_{+-} = 50$, $\Lambda_{+0} = 500$, $\lambda_{-0} = 5$, $f_+ = 5$, $f_- = 4$.

fraction of free ions in the sol increases as a function of concentration. This is due to the fact that the ion association probabilities for ions in the sol decrease after the gel point. Thus, the sol looks more and more like "dilute" electrolyte as we increase the overall salt concentration. For the parameters chosen in Fig. 6, we see that nearly all of the ions in the sol are free as we approach the pure salt limit. Though, this is a very small fraction of free ions overall because the electrolyte is nearly all gel. For model parameters more akin to an ionic liquid salt, we might expect a much larger fraction of free ions in the pure salt limit.[28]

Although, Fig. 6 demonstrates how clusters of overall size $(l+m)$ vary as a function a salt concentration, it does not tell us specifically how many anions or cations compose those clusters. That knowledge requires the use of the full bivariate probability distribution, α_{lm}, defined in Eq. (51), and plotted in Fig. 7 for various mole fractions of salt. We have chosen three different mole fractions of salt for plotting the distribution: $x = 0.08$ (pre-gel), $x = 0.17$ (near-gel), and $x = 0.44$ (post-gel). Both the pre-gel and near-gel distributions are skewed below the neutral cluster line (black dashed line), centered around the red solid line (denoting the most probable cluster of rank $l + m$). This indicates that clustered ions have a slight tendency to be negatively charged, containing more anions than cations. This effect is expected when the functionalities for ions are different. In this case, because the cations have a larger functionality than anions, each cation can accept more ion associations than each anion. Thus, there will be a tendency for there to be more anions in each cluster than cations.

Additionally, the cluster distribution is pushed toward larger clusters as the mole fraction is increased from 0.08 to 0.17 due to the increase in ionic association probability. However, as the mole fraction is increased to 0.44 (well above the gel point), the distribution is both pushed toward smaller clusters than at $x = 0.44$, as well as being skewed above the neutral cluster line, indicating that the finite clusters will on average more likely be positively charged. When the gel is formed, it absorbs many of the large negative clusters and is overall negatively charged. Therefore, the sol will have a net positive charge, leading to positively skewed cluster distribution.

We may probe the effect of solvent or salt type by tuning the different association constants, Λ_{ij}. If we assume that ion association sites are never empty (either occupied by solvent or counter-ions) and that the ions have equal functionality, we may use the "sticky symmetric ion approximation," which is outlined in the supplementary material. If we operate within the sticky symmetric ion approximation, we are left with one primary variable to manipulate: $\tilde{\Lambda} = \Lambda_{+-}/\Lambda_{+0}\Lambda_{-0}$. By varying $\tilde{\Lambda}$, we are tuning the "strength" of the electrolyte: weak electrolytes have $\tilde{\Lambda} \gg 1$ and strong electrolytes have $\tilde{\Lambda} \ll 1$. In Fig. 8, we display a pseudo-phase diagram of the most probable ionic "state" (either free, in a finite cluster, or in the ionic gel) of an ion as a function of $\tilde{\Lambda}$ and $\phi_\pm$. Note that Fig. 8 is generated within the sticky symmetric ion approximation and thus does not use the same parameters as Fig. 2 and Figs. 4–7. As was noted in Fig. 6 (left), free ions dominate at low salt fractions and gel dominates at moderately high salt fractions, with a narrow region of phase space where finite aggregates dominate. The critical gel boundary is denoted by the red dotted line, which generally resides within the

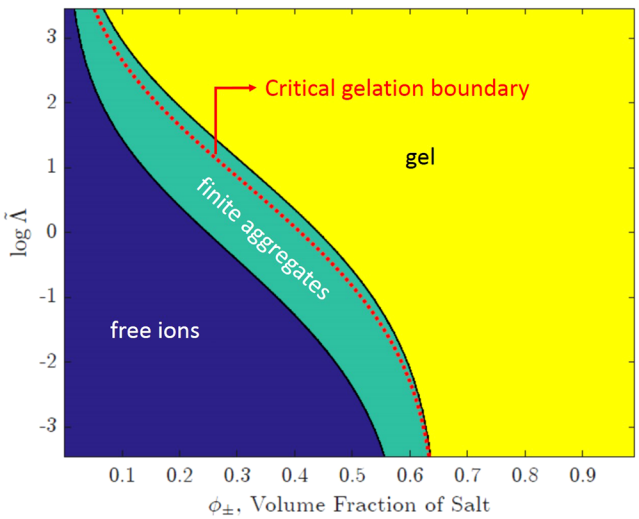

FIG. 8. A pseudo-phase diagram of the most probable ionic "state" (either free, in a finite cluster, or in the gel) as a function of $\tilde{\Lambda}$ and $\phi_\pm$. The red dotted line denotes the critical gel boundary. The diagram was generated within the sticky symmetric ion approximation (see supplementary material) for $\xi_+ = \xi_- = 5$ and $f_+ = f_- = 4$.

finite aggregate region of the phase diagram, because along the gel boundary, the fraction of ions within the gel will be infinitesimal. However, the gel tends to grow rapidly beyond the gel point by consuming larger ion clusters. Thus, the gel dominates the mixture soon after crossing the gel boundary. For $\ln(\tilde{\Lambda}) > 0$, the strength of the ion–ion attraction is more favorable than the ion–solvent interaction, which results in the onset of gelation occurring at smaller salt fractions. However, for $\ln(\tilde{\Lambda}) < 0$, the favorable ion–solvent interaction tends to "pull" free ions out of finite aggregates and gel, which pushes out the onset of gelation to larger salt fractions.

F. Toward the inclusion of excess electrostatic energy

On account of our various assumptions, principally our assumption of non-interacting clusters, the above developed model should not be applied to the entire range of salt concentrations but rather the moderate to super-concentrated regime. Other models may capture the behavior of electrolytes in the dilute to moderately concentrated regime.[60,61,70–72] This is further emphasized by the fact that our developed model does not recover Debye–Huckel behavior[73] in the dilute regime due to our neglect of the excess electrostatic energy of the electrolyte. Here, we will demonstrate how our theory can be augmented to recover Debye–Huckel theory in the dilute regime, which may potentially expand the concentration range (to include more dilute salt concentrations) within which our model is applicable.

As we have mentioned, our model of super-concentrated electrolytes treats the electrolyte as an ideal mixture of a polydisperse distribution of aggregates. In this way, clusters do not interact with each other, electrostatically or otherwise. However, charged clusters are expected to have electrostatic interactions with the surrounding medium, owing to the long range nature of electrostatics.

In principle, the free energy, originally written in Eq. (8), should include an additional term accounting for the excess electrostatic energy of the clusters (ΔF^{el}), written as follows:[74]

$$\beta\Delta F^* = \beta\sum_{lmsq}\left[e(l-m)N_{lmsq}\int_0^1 \Psi^0_{lmsq}(\lambda)\mathrm{d}\lambda\right], \tag{57}$$

where Ψ^0_{lmsq} is the mean-field electrostatic potential at the surface of a rank $lmsq$ cluster and λ is the charging parameter used in the Debye charging process. However, whereas all charged clusters may have excess electrostatic energy, free ions are expected to dominate the ionic strength of the electrolyte. Although charged clusters are permitted and expected in our model, they will generally be in relatively low concentrations and have a low charge to mass ratio. Thus, we expect that accounting for excess electrostatic energy of free ions will be the dominating contribution of the total excess electrostatic energy. The corresponding approximation reads

$$\begin{aligned}\beta\Delta F^* &\approx \beta\sum_{lmsq}\left[e(l-m)(\delta_{l,1}\delta_{m,0}+\delta_{l,0}\delta_{m,1})N_{lmsq}\int_0^1 \Psi^0(\lambda)\mathrm{d}\lambda\right]\\ &= (\alpha_+ + \alpha_-)N_\pm\int_0^1 \Psi^0(\lambda)\mathrm{d}\lambda,\end{aligned} \tag{58}$$

where Ψ^0 is the electrostatic potential on the surface of a free ion, i.e., an ion that is not associated with a counter-ion but may be solvated to any degree. Thus, the Debye charging process will integrate over only the charges on the free ions with the assumption that we may charge the ions composing the clusters without incurring any excess electrostatic energy.

Ψ^0 can be approximated by solving the linearized Poisson–Boltzmann equation (Debye–Huckel approximation) for a spherical ion of radius $a_\pm$, screened by a medium with permittivity ε and a concentration of $(\alpha_+ + \alpha_-)N_\pm/V$ diffuse free ions, where α_+ and α_- are the fraction of free cations and anions, respectively. For monovalent free ions (with charge $e\lambda$), this procedure yields

$$\Psi^0(\lambda) = \frac{e\lambda}{4\pi\varepsilon_0\varepsilon a_\pm} - \frac{e\lambda\kappa(\lambda)}{4\pi\varepsilon_0\varepsilon(1+a_\pm\kappa(\lambda))}, \tag{59}$$

where ε is the permittivity of the medium, $a_\pm$ is the radius of a free ion, and κ is the inverse Debye Length. Equation (59) contains two terms. The first term is the so-called self-energy of the free ions, which results in an implicit solvation energy of the free ions. The second term is the interaction of the free ions with the surrounding free ion atmosphere. Thus, for free ions, our model contains both implicit and explicit solvation. The radius of the ion used in Eq. (59) must be that of a fully solvated ion to avoid a potential "double-counting" for solvation. Essentially, for free ions, we handle the first solvation shell explicitly via ion–solvent association but account for the outer solvation shells implicitly via the self-energy. Note that for simplicity, we have assumed that all free ions have the same radius, $a_\pm$, but this could be relaxed in principle. κ is a function of the concentration of free ions, which is why we write $\kappa = \kappa(\lambda)$,

$$\begin{aligned}\kappa(\lambda) &= \sqrt{\frac{\lambda^2 e^2 N_\pm(\alpha_+ + \alpha_-)}{\varepsilon_0\varepsilon k_B T V}}\\ &= \lambda\kappa_0,\end{aligned} \tag{60}$$

where κ_0 is simply the inverse Debye length upon full charge of the free ions. Note that, for simplicity, we have made a strong assumption that $\varepsilon \neq \varepsilon(\lambda)$. Thus, ε does not change upon Debye charging the free ions, unlike in Ref. 71, but we will still allow it to be a function of the total volume fraction of salt, i.e., $\varepsilon = \varepsilon(\phi_\pm)$. In this case, the Debye charging process of the excess electrostatic energy free energy, ΔF^*,

$$\beta\Delta F^* = \frac{\beta(\alpha_+ + \alpha_-)N_\pm e^2}{8\pi\varepsilon_0\varepsilon a_\pm} + \frac{V}{4\pi a_\pm^3}\left[\ln(1+\kappa_0 a_\pm) - a_\pm\kappa_0 + \frac{a_\pm^2\kappa_0^2}{2}\right], \tag{61}$$

in which the first term is similar to the Born solvation energy and the second term is the classic Debye–Huckel result. This additional excess free energy term will affect the cluster equilibrium and thus the cluster distribution. Differentiating the free energy [Eq. (8)], including the excess electrostatic free energy [Eq. (61)], and establishing a cluster equilibrium results in the following cluster distribution:

$$K_{lmsq} = \exp\left(l+m+s+q-1-\Delta^\theta_{lmsq}-\Delta^*_{lmsq}\right), \tag{62}$$

where Δ^*_{lmsq} is the excess electrostatic free energy of formation of cluster rank $lmsq$ (derived explicitly in the supplementary material),

$$\Delta^*_{lmsq} = (l+m)(\delta_{m,1}\delta_{l,0}+\delta_{l,1}\delta_{m,0}-1)(\ln\gamma^{DH}_\pm + u^{Born}_\pm), \tag{63}$$

where $\gamma_{\pm}^{DH}$ is the Debye–Huckel activity coefficient,

$$\ln \gamma_{\pm}^{DH} = \frac{e^2}{8\pi k_B T \varepsilon_0 \varepsilon}\left(\frac{\kappa_0}{1 + a_{\pm}\kappa_0}\right), \tag{64}$$

and $u_{\pm}^{Born}$ is the dimensionless Born solvation energy for free ions,

$$u_{\pm}^{Born} = \frac{e^2}{8\pi k_B T \varepsilon_0 \varepsilon a_{\pm}}. \tag{65}$$

Note that the Born energy given by Eq. (65) is not defined in a conventional way–not as an absolute value of electrostatic free energy of transfer of an ion from vacuum to the liquid–but as electrostatic "self-energy" of an ion in the liquid. We may solve for the cluster distribution in the exact same manner as before, except with the new definition for the ionic association constant,

$$\Lambda_{+-} = \gamma_{\pm}^{DH} \exp(u_{\pm}^{Born})\Lambda_{+-}^{\theta}. \tag{66}$$

Note that $\gamma_{\pm}^{DH}$ and $u_{\pm}^{Born}$ are both functions of $\phi_{\pm}$ and p_{ij} via κ_0 and ε, altering the solution to the system of Eqs. (40) and (41).

Let us now compare the behavior of the model including and excluding the excess electrostatic free energy contribution. In Fig. 9, we plot the ionic association probabilities excluding excess electrostatics (blue curves), accounting for excess electrostatics with $\varepsilon = 80$ (red curves), and accounting for excess electrostatics with $\varepsilon = \varepsilon(\phi_{\pm})$ (yellow curves). For the salt concentration dependent permittivity, we employ a simple phenomenological interpolation model,

$$\varepsilon = \varepsilon_s \alpha_0 (1 - x) + \varepsilon_s^* (1 - \alpha_0)(1 - x) + \varepsilon_{\pm}^* (1 - \alpha_{\pm})x, \tag{67}$$

where x is the mole fraction of salt, α_0 is the fraction of the free solvent, ε_s is the permittivity of the pure solvent, ε_s^* is the dielectric constant contribution of the bound solvent, and $\varepsilon_{\pm}^*$ is the dielectric constant contribution of bound ions. Equation (67) is meant to be a simple interpolation formula in that ε changes from ε_s in the dilute regime to $\varepsilon_{\pm}^*$ as the solvent disappears and ions become more and more bound in clusters. We emphasize that this is not a linear interpolation between these limits as $\alpha_{\pm}$ and α_0 are highly nonlinear in overall salt concentration. For additional information on this permittivity formula, including a comparison of its concentration dependence with a typical empirical model, see Sec. III of the supplementary material.

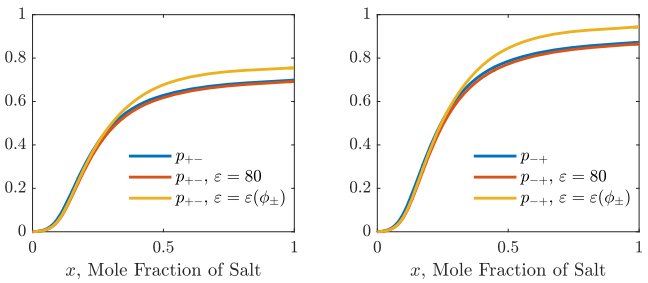

FIG. 9. A comparison of cation–anion association probability, p_{+-} (left), and anion–cation association probability, p_{-+} (right), when not accounting for excess electrostatic energy (blue), accounting for excess electrostatic energy with $\varepsilon = 80$ (red), and accounting for excess electrostatic energy with $\varepsilon = \varepsilon(\phi_{\pm})$ (yellow) with $\varepsilon_s = 78.4$, $\varepsilon_s^* = 10$, and $\varepsilon_{\pm}^*$. These curves are generated for $\xi_+ = 1$, $\xi_- = 10$, $\Lambda_{+-}^{\theta} = 50$, $\Lambda_{+0} = 500$, $\lambda_{-0} = 5$, $f_+ = 5$, $f_- = 4$.

Overall, we see that the ionic association is similar no matter if the excess electrostatic energy is included or not. Certainly, the constant permittivity model performs almost identically to the original model. Accounting for electrostatics with a variable permittivity leads to a slight deviation in association probability from the original model. This deviation stems mostly from the fact that $u_{\pm}^{Born}$ for free ions becomes very large at high salt concentrations (resulting from the decreasing permittivity), which drives the system equilibrium further toward the formation of clusters, as seen in Eq. (66). Overall, the exclusion of excess electrostatic energy, as in the original model, seems to be a reasonably justified approximation for modeling ionic association, but excess electrostatic energy can be included without an unreasonable increase in model complexity.

III. DISCUSSION

We have set forth a thermodynamic theory of superconcentrated electrolytes, in which we treat the electrolyte as a mixture of non-interacting, solvent-decorated ionic clusters. The most direct output of our theory is the distribution of clusters, which has already been discussed and displayed extensively in Sec. II E. However, our model can be useful beyond the determination of the cluster distribution. In this section, we discuss the major thermodynamic, transport, and rheological implications of our theory.

A. Thermodynamic implications

Our theory can also be used to predict some important thermodynamic quantities, such as the activity coefficients of species in the mixture. In Eq. (9), we wrote the chemical potential of a cluster of rank *lmsq*. The equilibrium condition [Eq. (17)] implies that the chemical potential of species in the cluster will be equal to their bare counterparts. Thus, we may write the chemical potential of an ion or solvent molecule as simply the chemical potential of a bare ion or solvent molecule. There is also an additional contribution associated with the excess electrostatic contribution to the free energy [Eq. (61)] for both ions ($\log \gamma_{\pm}^*$) and solvent ($\log \gamma_0^*$), which are derived explicitly in the supplementary material,

$$\beta\Delta\mu_+ = \beta\Delta\mu_{1000} = \ln(\phi_{1000}) + \xi_+(1 - c_{tot} + \phi_0 d) + \log \gamma_{\pm}^*, \tag{68}$$

$$\beta\Delta\mu_- = \beta\Delta\mu_{0100} = \ln(\phi_{0100})\xi_-(1 - c_{tot} + \phi_0 d) + \log \gamma_{\pm}^*, \tag{69}$$

$$\beta\Delta\mu_0 = \beta\Delta\mu_{0010} = \ln \phi_{0010} + 1 - c_{tot} + \phi_{\pm} d + \log \gamma_0^*. \tag{70}$$

We may derive ionic activity coefficients (with respect to a dilute solution reference state) by obtaining the excess part of the chemical potential. First, we must subtract off ideal entropy of mixing terms ($\ln \phi_i$). Then, we must subtract off the excess part of the chemical potential of the ions in the dilute limit, obtaining

$$\ln \gamma_{\pm} = \beta\Delta\mu_{\pm} - \ln\left\{\phi_{+,-}(1 - p_{\pm\mp}^{\circ} - p_{\pm 0}^{\circ})^{f_{\pm}}\right\} - (1 - \xi_{\pm} c_{tot}^{\circ}) - \xi_{\pm}\phi_0 d^{\circ}, \tag{71}$$

where the "$\circ$" superscript denotes the dilute limit (as salt concentration approaches 0) and $\phi_{+,-}$ denotes ϕ_+ or ϕ_- (not to be confused with $\phi_{\pm}$, the volume fraction of salt). The limiting ionic association probabilities, $p_{\pm\mp}^{\circ}$, tend toward 0. However, the limiting ion–solvent association probabilities, $p_{\pm 0}^{\circ}$, tend toward $\Lambda_{\pm 0}/(\Lambda_{\pm 0} + 1)$. Thus, if $\Lambda_{\pm 0} \gg 1$, we would expect ions to be fully associated with water in

the dilute limit. Similarly, the total dimensionless concentration, c^0_{tot}, tends toward 1, and d is zero before the gel point. We can then write the ionic activity coefficient as

$$\ln \gamma_\pm = f_\pm \ln\left\{(1 - p_{\pm\mp} - p_{\pm 0})(1 + \Lambda^\theta_{\pm 0})\right\} + \xi_\pm(1 - c_{tot} + \phi_0 d) + \log \gamma^*_\pm. \quad (72)$$

Similarly, we may write the activity coefficient of solvent molecules as

$$\ln \gamma_0 = \ln(1 - p_{0+} - p_{0-}) + 1 - c_{tot} + \phi_\pm d + \log \gamma^*_0. \quad (73)$$

It is also useful to define a mean ionic activity coefficient, $\bar{\gamma}_\pm = (\gamma_+\gamma_-)^{1/2}$, which is the more experimentally accessible quantity.

In Fig. 10, we plot the mean ionic activity coefficient, as well as that of the solvent, as a function of the volume fraction of salt. A fairly general prediction of our model, which is shown in Fig. 10, is that the activity of the salt tends to rise extraordinarily as a function of concentration, while that of the solvent simultaneously decreases. The salt activity increases for two primary reasons. First, the magnitude of the Born solvation energy of free ions increases due to the decrease in the dielectric constant of the electrolyte; free ions become more active in lower dielectric constant fluids. Second, ions become more paired with counter-ions as opposed to the solvent, which is unfavorable entropically, as well as enthalpically, for very strongly hydrating solvents. At the same time, the solvent activity tends to decrease at high salt concentrations due to the increase in the fraction of solvent that is favorably incorporated within the hydration shell of ions.

These trends in salt and solvent activity are interesting because one of the primary reasons water-in-salt electrolytes (WiSEs), in particular, have garnered so much interest is their ability to form a passivating solid|electrolyte interface (SEI) at the negative electrode in lithium-ion batteries (LIBs). This SEI layer suppresses the deleterious hydrogen evolution reaction, which prevents the use of dilute aqueous electrolytes in LIBs. Specifically, at the negative electrode, the solvent, in this case water, will not be stable to large electrode polarizations and will be spontaneously reduced to form hydrogen. When an SEI layer is present, the water does not come into direct contact with the electrode; thus, its electrochemical decomposition is suppressed. Therefore, it is desirable to form a stable SEI layer to prevent the electrochemical decomposition of the solvent. The SEI layer on an anode in contact with a WiSE would consist of reduction products involving the salt. By raising the activity of the salt (the reactant), the reduction potential of the salt is increased, and the overall driving force to form an SEI is increased. Similarly, by lowering the activity of the solvent (the reactant), the reduction potential of water is decreased, and the overall driving force to evolve hydrogen is decreased. Thus, by increasing salt concentration, the affinity to form an SEI layer is expected to increase and that to evolve hydrogen is expected to decrease, as observed experimentally.[11] At some salt concentration, there is likely a crossover, where it becomes more favorable to form an SEI layer than to evolve hydrogen. Because our model can capture the trends in activity for both ions and the solvent, it could potentially help predict when this crossover might occur and how it might change for different electrolyte materials.

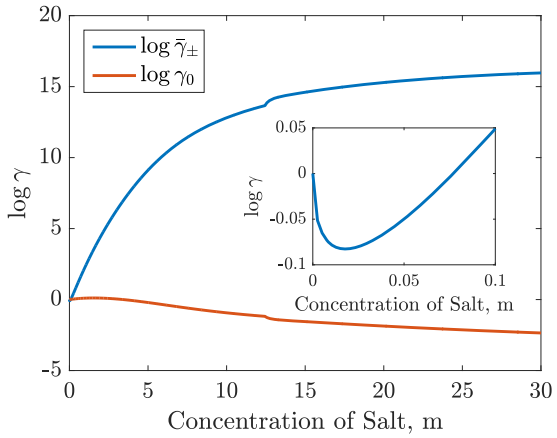

FIG. 10. The activity coefficients of the salt and solvent are plotted against the mole fraction of salt. These curves are generated for $\xi_+ = 1$, $\xi_- = 10$, $\Lambda_{+-} = 50$, $\Lambda_{+0} = 500$, $\lambda_{-0} = 5$, $f_+ = 5$, $f_- = 4$.

B. Transport implications

Although our model does not include any dynamics, we can begin to speculate on how certain transport properties, such as conductivity or ion transference numbers, may be influenced by ion association in the super-concentrated regime. For transport in multi-component, concentrated mixtures, it is often necessary to consider coupled diffusive fluxes,[75–77] which are related to the vector of species chemical potential gradients through the Onsager linear-response tensor or, after transformation to concentration gradients, the Stefan–Maxwell diffusivity tensor. This mathematical framework is the basis for concentrated solution theories of electrolyte transport,[78] which have been widely applied to batteries[79,80] and fitted to experiments[81–83] and molecular simulations.[84] The Stefan–Maxell formulation has also been extended to charged electrolytes in double layers.[85,86] Even for moderately concentrated electrolytes, however, the diffusivity tensor and ionic activity coefficients are fitted to experimental data with little theoretical guidance, and complex many-body interactions with solvent at high concentration are neglected. Our statistical model could provide a detailed, microscopic basis to model coupled fluxes in superconcentrated electrolytes as originating from the presence of ionic clusters.

Remarkably, as a result of the ion clustering predicted by our model, superconcentrated electrolytes may behave more like dilute electrolytes in that low concentrations of mobile charge carrier drift and diffuse with nearly independent fluxes. As such, for an associative mixture of ions, Ref. 38 proposed a modified Nernst–Einstein equation for conductivity, σ,

$$\sigma = \frac{e^2 c_{salt}}{k_B T} \sum_{lm} (l - m)^2 \alpha_{lm} D_{lm}, \quad (74)$$

where D_{lm} is the diffusivity of a cluster of rank lm, and the factor of $(l - m)^2$ arises because $l - m$ is the valence charge of a cluster of rank lm. Our model is able to predict the cluster fractions, α_{lm}, (as in Fig. 7) for different electrolyte compositions and temperatures, which could be extremely helpful when designing more conductive electrolytes. However, the cluster diffusivities, D_{lm}, would still be unknown, although they would undoubtedly decrease with the

increase in cluster size. As detailed in Refs. 38, 42, and 43, the contribution of clusters to the ionic current may be largely responsible for the very interesting observation of negative transference numbers for species in IL mixtures and solid-state electrolytes [see Eq. (5) of Ref. 38]. Though, for binary liquid electrolytes, we would not expect such exotic observations in ion transference numbers. Along the same vein, observations of negative Stefan–Maxwell diffusion coefficients[87,88] have been reported for ion transport of concentrated electrolytes through membranes, which may be due to ion clustering.

Although there are likely systems in which ion clusters play a large role in conducting ionic current, recent work in Ref. 28 found that free ions ($l + m = 1$) are the major contributor to ionic current in neat ionic liquids. In that case, conductivity obeys an even simpler equation

$$\sigma = \frac{e^2 c_{salt}}{k_B T}(\alpha_+ D_+ + \alpha_- D_-), \tag{75}$$

where $\alpha_+ = (1-p_{+-})^{f_+}$ is the fraction of free cations, $\alpha_- = (1-p_{-+})^{f_-}$ is the fraction of free anions, and $D_\pm$ is the diffusivity of the free cation or anion. The ability to use Eq. (75) instead of (74) depends on if we can neglect the cluster contribution to the ionic strength of the electrolyte. Our model allows us to predict the ionic strength and decompose the respective contributions from free ions and clusters. In the left panel of Fig. 11, we plot the dimensionless ionic strength (non-dimensionalized by the overall salt concentration). The dashed line in Fig. 11 represents the free ion contribution to the ionic strength, while the solid curve represents the total ionic strength. It is apparent that free ions dominate the ionic strength of the electrolyte no matter the salt concentration, at least for the model parameters given in the caption. There is a small region where there is a perceptible contribution of ion clusters to the ionic strength, which corresponds to concentrations very close to the gel point of the electrolyte ($x = 0.18$). Nonetheless, it appears as if Eq. (75) could suffice for modeling the conductivity of our fictional electrolyte.

Within our model, the concentration of free ions can display nonlinear or even non-monotonic behavior as a function of overall salt concentration. At high concentrations, adding more salt can, in fact, decrease the number of free ions in solution. This is shown in Fig. 11, where we have plotted the concentration of free ions as a function of the mole fraction of salt. Here, we have used the parameters listed in the caption to generate the curves, which are the same parameters that have been used for the majority of the paper. The non-monotonic concentration of free ions is likely largely responsible for the non-monotonic ionic conductivity that has been widely observed for concentrated electrolytes[89] or IL-solvent mixtures.[90–92] Though, we must note that $D_\pm$ is also expected to have a large role in the concentration dependence of ionic conductivity.

One interesting aspect of this model is that for asymmetrically associating ions, we obtain different fractions of free anions and cations, as shown in Fig. 11. If the free anions and cations have equivalent diffusivities, then we can write the transference number as

$$t_\pm = \frac{\alpha_\pm}{\alpha_+ + \alpha_-}. \tag{76}$$

Thus, assuming free ions are the dominant carrier of charge, our model would predict asymmetric transference numbers ($t_\pm \neq 0.5$) for salts with ions that do not have equivalent functionalities, as shown in the inset of Fig. 11. In general, for binary mixtures of monovalent salts, the ion with more association sites will have a higher fraction of free ions than the ion with less association sites. The reason for this is quite subtle. Ultimately, when $f_+ > f_-$, for a fixed number of ion–counter-ion associations, the cations need less molecules to form those associations than anions. Thus, more cations will be free than anions, and we would observe that $t_+ > 0.5$ and $t_- < 0.5$. The opposite would be true for the electrolyte if $f_- > f_+$.

C. Rheological implications

Gel-forming electrolytes should display intriguing viscoelastic properties. In polymers, typically the presence of gel is detected by probing the rheology of the mixture. At the gel point, the viscosity is expected to diverge and the equilibrium shear modulus is expected to become finite.[65] Because our gel is composed of reversible physical associations between ions, we do not expect the viscosity to

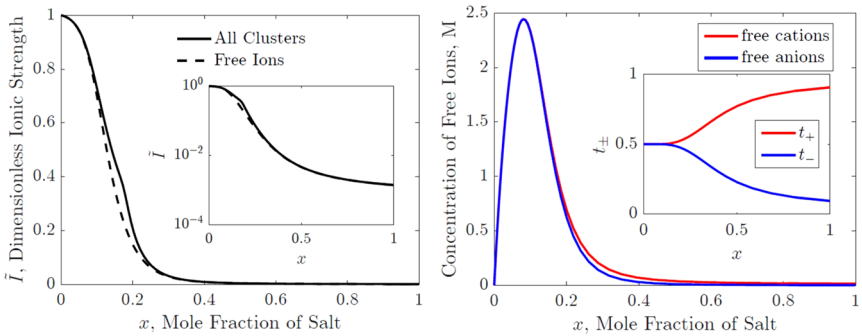

FIG. 11. (Left) A plot of the dimensionless ionic strength as a function of the mole fraction of salt when account for all charged clusters (solid line) or just free ions (dashed line). The inset of the left panel displays the same curves on a log–log plot to visualize better the high mole fraction regime. (Right) The concentration of free anions and cations is plotted against the mole fraction of salt, displaying non-monotonic salt concentration dependence. Within the inset of the right panel, the transference number of anions (t_-) and cations (t_+) is plotted against the mole fraction of salt according to Eq. (76). These curves are generated for $\xi_+ = 1$, $\xi_- = 10$, $\Lambda_{+-} = 50$, $\Lambda_{+0} = 500$, $\lambda_{-0} = 5$, $f_+ = 5$, $f_- = 4$.

formally diverge. Nonetheless, thermoreversible gels should display a finite shear modulus. Flory related the equilibrium shear modulus, G_e, to the fraction of the gel in the mixture for tetrafunctional associating polymer strands.[65] This was later extended for any f functional associating polymer strand by Nijenhuis. This extension would be applicable for our case of ion gels if the ions have the equal functionalities, f,

$$G_e = -2cRT\left(\frac{\ln w_{\pm}^{sol}}{1-w_{\pm}^{sol}} \cdot \frac{1-(w_{\pm}^{sol})^{f/2}}{1-(w_{\pm}^{sol})^{f/2-1}} \cdot \frac{f-2}{f} + 1\right)(1-w_{\pm}^{sol}), \quad (77)$$

where c is the molar concentration of salt and R is the gas constant. Equation (77) predicts, as expected, that G_e will be zero prior to the formation of gel and then increase with the increase in gel fraction. If we again operate within the sticky symmetric ion approximation, then we can see how the equilibrium shear modulus is modulated by the electrolyte concentration (via $\phi_{\pm}$) and strength (via $\tilde{\Lambda}$).

In Fig. 12, we display a contour map of the equilibrium shear modulus using Eq. (77) as functions of $\phi_{\pm}$ and $\log\tilde{\Lambda}$. The shear modulus is predictably zero (white region), when there is no ionic gel present in the electrolyte, and becomes finite beyond the gel point. Additionally, the shear modulus increases monotonically with the increase in gel fraction. As such, it increases with concentration but tends to decrease as the electrolyte becomes weaker ($\log\Lambda$ decreases). There is a subtlety to this statement, as can be seen by the non-monotonicity in the contours of G_e at high salt concentrations. For very strong electrolytes ($\log\tilde{\Lambda} < 2$) and for a given volume fraction of salt that is beyond the gel boundary, by increasing $\tilde{\Lambda}$ (increasing the affinity for ion association), the gel fraction, in fact, decreases. This is counter-intuitive because we would expect more gel when the affinity for ion association is stronger. However, within the gel, the model allows for intra-cluster loops (defined as a closed path that is formed from traversing bonds in a cluster). Increasing the affinity for ion association induces more intracluster loops, which frees up ions from the gel while simultaneously containing more ion–counter-ion associations. Thus, in this regime, increasing the affinity for ion association decreases the shear modulus.

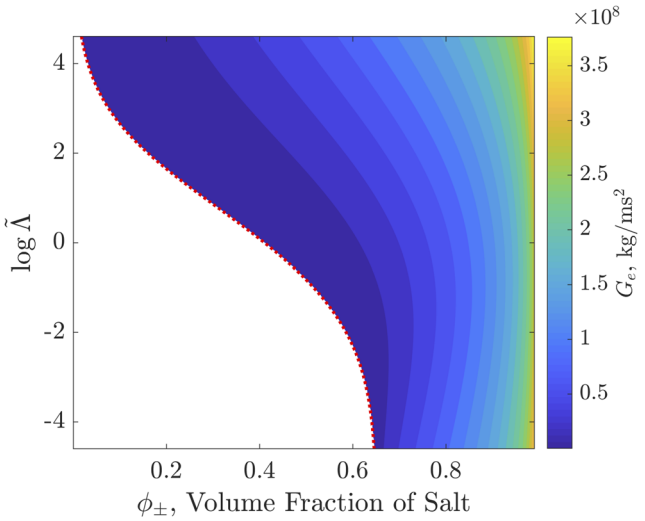

FIG. 12. A contour map of the equilibrium shear modulus, G_e, as a function of $\tilde{\Lambda}$ and $\phi_{\pm}$. The red dotted line denotes the critical gel boundary. The region of white denotes the pre-gel region, where the equilibrium shear modulus is exactly 0. The diagram was generated within the sticky symmetric ion approximation (see supplementary material) for $\xi_+ = \xi_- = 5$ and $f_+ = f_- = 4$.

This subtlety should not obscure the result that when an ionic gel is present, the mixture may display viscoelastic properties. Interestingly, viscoelastic properties have indeed been observed experimentally for some common imidizolium-based ILs.[93] In that work, the equilibrium shear modulus of elasticity decreases as a function of temperature, which would be consistent with the melting and destruction of an ionic gel.

There is limited literature on this topic, however. Furthermore, Ref. 93 does not attempt to compute a gel point. Perhaps, the most reliable method for determining the exact gel point was introduced by Winter and Chambon.[94] They determined the gel point to occur at the intersection of the dynamic loss and the storage moduli for an oscillatory shear experiment. This could be a route to experimentally probe gelation in concentrated electrolytes.

IV. CONCLUSION

Here, we have cast the mean-field theory of thermoreversible association and gelation from polymer physics into the context of electrolytes. The presented theory allows complicated, branched ionic aggregates to be included in models of concentrated electrolytes. Previously, only ion pairs and occasionally ion triplets were included in models of ionic association for concentrated electrolytes. However, these models break down when the system becomes sufficiently concentrated, which motivated the presented theory. More specifically, we developed a model for aggregation and gelation between cations, anions, and solvent molecules, with alternating cation–anion aggregates/gel and solvent molecules decorating this "ionic backbone."

The theory can describe the cluster composition of an electrolyte as a function of salt concentration (or temperature), where different ionic states (free, aggregated, or gelled) dominate depending on the conditions. Higher salt concentrations favor the formation of a percolating gel, while low salt concentrations tend to have only free ions; between these extremes exists a narrow domain where finite aggregates dominate in the electrolyte.

We expect that our model will have implications for the bulk thermodynamic, transport, and rheological properties of super-concentrated electrolytes, which can be probed experimentally and used to guide the design of these dense ionic fluids.

The developed theory is best applied to super-concentrated electrolytes with "complicated" ions, where crystalline solids cannot precipitate out. This includes neat ionic liquids, water-in-salt electrolytes, ionic liquid-solvent mixtures, or hydrate melts, which are highly relevant for battery or super-capacitor applications. Often super-concentrated electrolytes contain bulky, asymmetric ions that lead to high solubility and low melting points of the salts. Asymmetric ions in ILs have been shown to exhibit preferential orientations from density functional theory (DFT).[57] Moreover, some ILs can, in fact, form hydrogen bonds between ions, permitting strong and well-defined bonds between ions.[57] Therefore, our assumption of a fixed functionality for each ion might be justified for super-concentrated electrolytes, where such asymmetric ions are common.

The ion aggregates that are formed in these systems tend to be irregular and disordered, which is quite consistent with our approximation of Cayley tree-like ion aggregates. Inorganic salts, such as NaCl, form aggregates that may be ordered and semi-crystalline, as opposed to the branched structures that are characteristic of Cayley trees. Ordered aggregates nucleate, phase separate, and induce the precipitation of crystalline salt, without forming a gel. In these types of systems, the physics of ion gelation would probably not be as relevant, and our description of ion aggregation would be flawed. Nonetheless, we expect that our model is well-equipped for capturing the ion association, solvation, and gelation in super-concentrated electrolytes.

It may be possible to extend our approach to interfacial properties as well. Specifically, it has already been shown that understanding the partitioning of ions[27,32,95] and solvent[96] between free and bound states is extremely enlightening in modeling the electrical double layer (EDL) of ionic liquids and WiSE's. Our model provides a more detailed and generalized picture of the states of ions or solvent, which may be leveraged to develop more accurate and general models of the EDL. EDL properties will also influence electrokinetic phenomena and may help explain many puzzling observations, such as flow reversals in concentrated electrolytes.[97,98] As with polymers under confinement, it will also be interesting to extend our model to nanopores, where cluster sizes are influenced by geometrical constraints.

SUPPLEMENTARY MATERIAL

See the supplementary material for (1) model results with alternate chosen parameters, (2) derivation of the "sticky cation approximation," and (3) more information and derivations concerning the excess electrostatic energy of the electrolyte.

ACKNOWLEDGMENTS

The authors would like to thank J. Pedro de Souza, Tzyy-shang Lin, and Guang Feng for helpful discussions. The authors would like to acknowledge the Imperial College-MIT seed fund. M.M. and M.Z.B. acknowledge support from a Amar G. Bose Research Grant. Z.A.H.G was supported through a studentship in the Centre for Doctoral Training on Theory and Simulation of Materials at Imperial College London funded by the EPSRC (Grant No. EP/L015579/1) and from the Thomas Young Centre under Grant No. TYC-101. S.B. was also supported by the National Natural Science Foundation of China (Grant No. 51876072) and acknowledges the financial support from the China Scholarship Council. A.A.K. would like to acknowledge the research grant by the Leverhulme Trust (Grant No. RPG-2016- 223).

DATA AVAILABILITY

Data sharing is not applicable to this article as no new data were created or analyzed in this study.

REFERENCES

[1] H. S. Harned, B. B. Owen, and C. V. King, "The physical chemistry of electrolytic solutions," J. Electrochem. Soc. **106**, 15C (1959).
[2] J. Zwanikken and R. van Roij, "Inflation of the screening length induced by Bjerrum pairs," J. Phys.: Condens. Matter **21**, 424102 (2009).
[3] N. Bjerrum, "Kgl. danske vid. selskab," Math.-Fys. Medd. **7**, 1–48 (1926).
[4] Y. Marcus and G. Hefter, "Ion pairing," Chem. Rev. **106**, 4585–4621 (2006).
[5] C. A. Kraus and R. M. Fuoss, "Properties of electrolytic solutions. I. Conductance as influenced by the dielectric constant of the solvent medium," J. Am. Chem. Soc. **55**, 21–36 (1933).
[6] R. M. Fuoss and C. A. Kraus, "Properties of electrolytic solutions. IV. The conductance minimum and the formation of triple ions due to the action of Coulomb forces," J. Am. Chem. Soc. **55**, 2387–2399 (1933).
[7] R. M. Fuoss and C. A. Kraus, "Properties of electrolytic solutions. IX. Conductance of some salts in benzene," J. Am. Chem. Soc. **55**, 3614–3620 (1933).
[8] J. Barthel, H. Krienke, M. Holovko, V. Kapko, and I. Protsykevich, "The application of the associative mean spherical approximation in the theory of nonaqueous electrolyte solutions," Condens. Matter Phys. **3**, 657 (2000).
[9] L. Suo, Y.-S. Hu, H. Li, M. Armand, and L. Chen, "A new class of solvent-in-salt electrolyte for high-energy rechargeable metallic lithium batteries," Nat. Commun. **4**, 1481 (2013).
[10] K. Sodeyama, Y. Yamada, K. Aikawa, A. Yamada, and Y. Tateyama, "Sacrificial anion reduction mechanism for electrochemical stability improvement in highly concentrated Li-salt electrolyte," J. Phys. Chem. C **118**, 14091–14097 (2014).
[11] L. Suo, O. Borodin, T. Gao, M. Olguin, J. Ho, X. Fan, C. Luo, C. Wang, and K. Xu, ""Water-in-salt" electrolyte enables high-voltage aqueous lithium-ion chemistries," Science **350**, 938–943 (2015).
[12] L. Smith and B. Dunn, "Opening the window for aqueous electrolytes," Science **350**, 918 (2015).
[13] Y. Yamada, K. Usui, K. Sodeyama, S. Ko, Y. Tateyama, and A. Yamada, "Hydrate-melt electrolytes for high-energy-density aqueous batteries," Nat. Energy **1**, 16129 (2016).
[14] J. Wang, Y. Yamada, K. Sodeyama, C. H. Chiang, Y. Tateyama, and A. Yamada, "Superconcentrated electrolytes for a high-voltage lithium-ion battery," Nat. Commun. **7**, 12032 (2016).
[15] A. Gambou-Bosca and D. Bélanger, "Electrochemical characterization of MnO_2-based composite in the presence of salt-in-water and water-in-salt electrolytes as electrode for electrochemical capacitors," J. Power Sources **326**, 595 (2016).
[16] W. Sun, L. Suo, F. Wang, N. Eidson, C. Yang, F. Han, Z. Ma, T. Gao, M. Zhu, and C. Wang, ""Water-in-Salt" electrolyte enabled $LiMn_2O_4/TiS_2$ Lithium-ion batteries," Electrochem. Commun. **82**, 71–74 (2017).
[17] L. Suo, O. Borodin, Y. Wang, X. Rong, W. Sun, X. Fan, S. Xu, M. A. Schroeder, A. V. Cresce, F. Wang *et al.*, ""water-in-salt" electrolyte makes aqueous sodium-ion battery safe, green, and long-lasting," Adv. Energy Mater. **7**, 1701189 (2017).
[18] X. Dong, H. Yu, Y. Ma, J. L. Bao, D. G. ruhlar, Y. Wang, and Y. Xia, "All-Organic rechargeable battery with reversibility supported by "water-in-salt" electrolyte," Chem. - A Eur. J. **23**, 2560 (2017).
[19] K. M. Diederichsen, E. J. McShane, and B. D. McCloskey, "Promising routes to a high Li^+ transference number electrolyte for lithium ion batteries," ACS Energy Lett. **2**, 2563 (2017).
[20] C. Yang, J. Chen, T. Qing, X. Fan, W. Sun, A. von Cresce, M. S. Ding, O. Borodin, J. Vatamanu, M. A. Schroeder *et al.*, "4.0 V aqueous Li-ion batteries," Joule **1**, 122–132 (2017).
[21] C. Yang, L. Suo, O. Borodin, F. Wang, W. Sun, T. Gao, X. Fan, S. Hou, Z. Ma, K. Amine, K. Xu, and C. Wang, "Unique aqueous Li-ion/sulfur chemistry with high energy density and reversibility," Proc. Natl. Acad. Sci. U. S. A. **114**, 6197 (2017).
[22] F. Wang, O. Borodin, M. S. Ding, M. Gobet, J. Vatamanu, X. Fan, T. Gao, N. Eidson, Y. Liang, W. Sun *et al.*, "Hybrid aqueous/non-aqueous electrolyte for safe and high-energy Li-ion batteries," Joule **2**, 927–937 (2018).
[23] D. P. Leonard, Z. Wei, G. Chen, F. Du, and X. Ji, "Water-in-salt electrolyte for potassium-ion batteries," ACS Energy Lett. **3**, 373–374 (2018).
[24] C. Yang, J. Chen, X. Ji, T. P. Pollard, X. Lü, C. J. Sun, S. Hou, Q. Liu, C. Liu, T. Qing, Y. Wang, O. Borodin, Y. Ren, K. Xu, and C. Wang, "Aqueous Li-ion battery enabled by halogen conversion–intercalation chemistry in graphite," Nature **570**, 245–250 (2019).

[25]Q. Dou, Y. Lu, L. Su, X. Zhang, S. Lei, X. Bu, L. Liu, D. Xiao, J. Chen, S. Shi, and X. Yan, "A sodium perchlorate-based hybrid electrolyte with high salt-to-water molar ratio for safe 2.5 V carbon-based supercapacitor," Energy Storage Mater. **23**, 603 (2019).
[26]M. Chen, Z. A. H. Goodwin, G. Feng, and A. A. Kornyshev, "On the temperature dependence of the double layer capacitance of ionic liquids," J. Electroanal. Chem. **819**, 347–358 (2018).
[27]Z. A. H. Goodwin and A. A. Kornyshev, "Underscreening, overscreening and double-layer capacitance," Electrochem. Commun. **82**, 129–133 (2017).
[28]G. Feng, M. Chen, S. Bi, Z. A. Goodwin, E. B. Postnikov, N. Brilliantov, M. Urbakh, and A. A. Kornyshev, "Free and bound states of ions in ionic liquids, conductivity, and underscreening paradox," Phys. Rev. X **9**, 021024 (2019).
[29]M. A. Gebbie, M. Valtiner, X. Banquy, E. T. Fox, W. A. Henderson, and J. N. Israelachvili, "Ionic liquids behave as dilute electrolyte solutions," Proc. Natl. Acad. Sci. U. S. A. **110**, 9674–9679 (2013).
[30]M. A. Gebbie, H. A. Dobbs, M. Valtiner, and J. N. Israelachvili, "Long-range electrostatic screening in ionic liquids," Proc. Natl. Acad. Sci. U. S. A. **112**, 7432–7437 (2015).
[31]A. M. Smith, A. A. Lee, and S. Perkin, "The electrostatic screening length in concentrated electrolytes increases with concentration," J. Phys. Chem. Lett. **7**, 2157–2163 (2016).
[32]Z. A. H. Goodwin, G. Feng, and A. A. Kornyshev, "Mean-field theory of electrical double layer in ionic liquids with account of short-range correlations," Electrochim. Acta **225**, 190–197 (2017).
[33]S. Kim, H. Kim, J.-H. Choi, and M. Cho, "Ion aggregation in high salt solutions: Ion network versus ion cluster," J. Chem. Phys. **141**, 124510 (2014).
[34]J.-H. Choi and M. Cho, "Ion aggregation in high salt solutions. II. Spectral graph analysis of water hydrogen-bonding network and ion aggregate structures," J. Chem. Phys. **141**, 154502 (2014).
[35]J.-H. Choi and M. Cho, "Ion aggregation in high salt solutions. IV. Graph-theoretical analyses of ion aggregate structure and water hydrogen bonding network," J. Chem. Phys. **143**, 104110 (2015).
[36]J.-H. Choi, H. R. Choi, J. Jeon, and M. Cho, "Ion aggregation in high salt solutions. VII. The effect of cations on the structures of ion aggregates and water hydrogen-bonding network," J. Chem. Phys. **147**, 154107 (2017).
[37]O. Borodin, L. Suo, M. Gobet, X. Ren, F. Wang, A. Faraone, J. Peng, M. Olguin, M. Schroeder, M. S. Ding *et al.*, "Liquid structure with nano-heterogeneity promotes cationic transport in concentrated electrolytes," ACS Nano **11**, 10462–10471 (2017).
[38]A. France-Lanord and J. C. Grossman, "Correlations from ion pairing and the Nernst-Einstein equation," Phys. Rev. Lett. **122**, 136001 (2019).
[39]Z. Yu, L. A. Curtiss, R. E. Winans, T. Li, and L. Cheng, "Asymmetric composition of ionic aggregates and the origin of high correlated transference number in water-in-salt electrolytes," J. Phys. Chem. Lett. **11**, 1276 (2020).
[40]J. Lim, K. Park, H. Lee, J. Kim, K. Kwak, and M. Cho, "Nanometric water channels in water-in-salt lithium ion battery electrolyte," J. Am. Chem. Soc. **140**, 15661–15667 (2018).
[41]N. H. Lewis, Y. Zhang, B. Dereka, E. V. Carino, E. J. Maginn, and A. Tokmakoff, "Signatures of ion-pairing and aggregation in the vibrational spectroscopy of super-concentrated aqueous lithium bistriflimide solutions," J. Phys. Chem. C **124**, 3470 (2020).
[42]N. Molinari, J. P. Mailoa, N. Craig, J. Christensen, and B. Kozinsky, "Transport anomalies emerging from strong correlation in ionic liquid electrolytes," J. Power Sources **428**, 27–36 (2019).
[43]N. Molinari, J. P. Mailoa, and B. Kozinsky, "General trend of a negative Li effective charge in ionic liquid electrolytes," J. Phys. Chem. Lett. **10**, 2313–2319 (2019).
[44]P. J. Flory, "Molecular size distribution in three dimensional polymers. I. Gelation," J. Am. Chem. Soc. **63**, 3083–3090 (1941).
[45]P. J. Flory, "Constitution of three-dimensional polymers and the theory of gelation," J. Phys. Chem. **46**, 132–140 (1942).
[46]W. H. Stockmayer, "Theory of molecular size distribution and gel formation in branched-chain polymers," J. Chem. Phys. **11**, 45–55 (1943).
[47]W. H. Stockmayer, "Theory of molecular size distribution and gel formation in branched polymers II. General cross linking," J. Chem. Phys. **12**, 125–131 (1944).
[48]D. Stauffer and A. Aharony, *Introduction to Percolation Theory*, 2nd ed. (Taylor & Francis, London, 1994).
[49]F. Tanaka, "Theory of thermoreversible gelation," Macromolecules **22**, 1988–1994 (1989).
[50]F. Tanaka, "Thermodynamic theory of network-forming polymer solutions. 1," Macromolecules **23**, 3784–3789 (1990).
[51]F. Tanaka and W. H. Stockmayer, "Thermoreversible gelation with junctions of variable multiplicity," Macromolecules **27**, 3943–3954 (1994).
[52]F. Tanaka and M. Ishida, "Thermoreversible gelation of hydrated polymers," J. Chem. Soc., Faraday Trans. **91**, 2663–2670 (1995).
[53]M. Ishida and F. Tanaka, "Theoretical study of the postgel regime in thermoreversible gelation," Macromolecules **30**, 3900–3909 (1997).
[54]F. Tanaka, "Thermoreversible gelation of associating polymers," Physica A **257**, 245–255 (1998).
[55]F. Tanaka and M. Ishida, "Thermoreversible gelation with two-component networks," Macromolecules **32**, 1271–1283 (1999).
[56]F. Tanaka, "Theoretical study of molecular association and thermoreversible gelation in polymers," Polym. J. **34**, 479 (2002).
[57]P. A. Hunt, C. R. Ashworth, and R. P. Matthews, "Hydrogen bonding in ionic liquids," Chem. Soc. Rev. **44**, 1257 (2015).
[58]L. W. Bahe, "Structure in concentrated solutions of electrolytes. Field-dielectric-gradient forces and energies," J. Phys. Chem. **76**, 1062–1071 (1972).
[59]L. M. Varela, M. Garcia, F. Sarmiento, D. Attwood, and V. Mosquera, "Pseudolattice theory of strong electrolyte solutions," J. Chem. Phys. **107**, 6415–6419 (1997).
[60]W. Ebeling and M. Grigo, "An analytical calculation of the equation of state and the critical point in a dense classical fluid of charged hard spheres," Ann. Phys. **492**, 21–30 (1980).
[61]Y. Levin and M. E. Fisher, "Criticality in the hard-sphere ionic fluid," Physica A **225**, 164–220 (1996).
[62]A. A. Lee, D. Vella, S. Perkin, and A. Goriely, "Are room-temperature ionic liquids dilute electrolytes?," J. Phys. Chem. Lett. **6**, 159–163 (2014).
[63]A. Levy, M. McEldrew, and M. Z. Bazant, "Spin-glass charge ordering in ionic liquids," Phys. Rev. Mater. **3**, 055606 (2019).
[64]P. J. Flory, "Thermodynamics of high polymer solutions," J. Chem. Phys. **10**, 51–61 (1942).
[65]P. J. Flory, *Principles of Polymer Chemistry* (Cornell University Press, 1953).
[66]W. H. Stockmayer, "Molecular distribution in condensation polymers," J. Polym. Sci. **9**, 69–71 (1952).
[67]A. Matsuyama and F. Tanaka, "Theory of solvation-induced reentrant phase separation in polymer solutions," Phys. Rev. Lett. **65**, 341 (1990).
[68]F. Tanaka, *Polymer Physics: Applications to Molecular Association and Thermoreversible Gelation* (Cambridge University Press, 2011).
[69]C. W. Macosko and D. R. Miller, "A new derivation of average molecular weights of nonlinear polymers," Macromolecules **9**, 199–206 (1976).
[70]J. Vincze, M. Valiskó, and D. Boda, "The nonmonotonic concentration dependence of the mean activity coefficient of electrolytes is a result of a balance between solvation and ion-ion correlations," J. Chem. Phys. **133**, 154507 (2010).
[71]I. Y. Shilov and A. K. Lyashchenko, "The role of concentration dependent static permittivity of electrolyte solutions in the Debye–Huckel theory," J. Phys. Chem. B **119**, 10087–10095 (2015).
[72]A. Levy, M. Bazant, and A. Kornyshev, "Ionic activity in concentrated electrolytes: Solvent structure effect revisited," Chem. Phys. Lett. **738**, 136915 (2020).
[73]P. Debye and E. Hückel, "The theory of electrolytes. I. Freezing point depression and related phenomena [zur theorie der elektrolyte. I. Gefrierpunktserniedrigung und verwandte erscheinungen]," Phys. Z. **24**, 185–206 (1923).
[74]R. Fowler and E. Guggenheim, *Statistical Thermodynamics* (Cambridge University Press, 1939).
[75]S. R. De Groot and P. Mazur, *Non-equilibrium Thermodynamics* (Courier Corporation, 2013).
[76]R. Krishna and J. A. Wesselingh, "The Maxwell-Stefan approach to mass transfer," Chem. Eng. Sci. **52**, 861–911 (1997).

[77]W. M. Deen, *Analysis of Transport Phenomena* (Oxford University Press, 1998).
[78]J. Newman and K. E. Thomas-Alyea, *Electrochemical Systems* (John Wiley & Sons, 2012).
[79]R. B. Smith and M. Z. Bazant, "Multiphase porous electrode theory," J. Electrochem. Soc. **164**, E3291–E3310 (2017).
[80]K. Thomas, R. Darling, and J. Newman, *Advances in Lithium-Ion Batteries*, edited by W. van Schalkwijk and B. Scrosati (Kluwer Academic/Plenum Publishers, 2002).
[81]L. O. Valøen and J. N. Reimers, "Transport properties of $LiPF_6$-based Li-ion battery electrolytes," J. Electrochem. Soc. **152**, A882–A891 (2005).
[82]A. Nyman, M. Behm, and G. Lindbergh, "Electrochemical characterisation and modelling of the mass transport phenomena in $LiPF_6$–EC–EMC electrolyte," Electrochim. Acta **53**, 6356–6365 (2008).
[83]H. Lundgren, M. Behm, and G. Lindbergh, "Electrochemical characterization and temperature dependency of mass-transport properties of $LiPF_6$ in EC:DEC," J. Electrochem. Soc. **162**, A413–A420 (2015).
[84]D. R. Wheeler and J. Newman, "Molecular dynamics simulations of multicomponent diffusion. 1. Equilibrium method," J. Phys. Chem. B **108**, 18353–18361 (2004).
[85]S. T. P. Psaltis and T. W. Farrell, "Comparing charge transport predictions for a ternary electrolyte using the Maxwell–Stefan and Nernst–Planck equations," J. Electrochem. Soc. **158**, A33–A42 (2011).
[86]B. Balu and A. S. Khair, "Role of Stefan–Maxwell fluxes in the dynamics of concentrated electrolytes," Soft Matter **14**, 8267–8275 (2018).
[87]G. Kraaijeveld and J. A. Wesselingh, "Negative Maxwell-Stefan diffusion coefficients," Ind. Eng. Chem. Res. **32**, 738–742 (1993).
[88]J. A. Wesselingh, P. Vonk, and G. Kraaijeveld, "Exploring the Maxwell-Stefan description of ion exchange," Chem. Eng. J. Biochem. Eng. J. **57**, 75–89 (1995).
[89]V. M. Lobo and J. Quaresma, *Handbook of electrolyte solutions*, Physical sciences data (Elsevier, 1989), Vol. 41.
[90]A. Stoppa, J. Hunger, and R. Buchner, "Conductivities of binary mixtures of ionic liquids with polar solvents," J. Chem. Eng. Data **54**, 472–479 (2009).
[91]W. Li, Z. Zhang, B. Han, S. Hu, Y. Xie, and G. Yang, "Effect of water and organic solvents on the ionic dissociation of ionic liquids," J. Phys. Chem. B **111**, 6452–6456 (2007).
[92]V. V. Chaban, I. V. Voroshylova, O. N. Kalugin, and O. V. Prezhdo, "Acetonitrile boosts conductivity of imidazolium ionic liquids," J. Phys. Chem. B **116**, 7719–7727 (2012).
[93]W. Makino, R. Kishikawa, M. Mizoshiri, S. Takeda, and M. Yao, "Viscoelastic properties of room temperature ionic liquids," J. Chem. Phys. **129**, 104510 (2008).
[94]H. H. Winter and F. Chambon, "Analysis of linear viscoelasticity of a crosslinking polymer at the gel point," J. Rheol. **30**, 367–382 (1986).
[95]Y. Avni, R. M. Adar, and D. Andelman, "Charge oscillations in ionic liquids: A microscopic cluster model," Phys. Rev. E **101**, 010601 (2020).
[96]M. McEldrew, Z. A. H. Goodwin, A. A. Kornyshev, and M. Z. Bazant, "Theory of the double layer in water-in-salt electrolytes," J. Phys. Chem. Lett. **9**, 5840–5846 (2018).
[97]M. Z. Bazant, M. S. Kilic, B. D. Storey, and A. Ajdari, "Towards an understanding of nonlinear electrokinetics at large voltages in concentrated solutions," Adv. Colloid Interface Sci. **152**, 48–88 (2009).
[98]B. D. Storey and M. Z. Bazant, "Effects of electrostatic correlations on electrokinetic phenomena," Phys. Rev. E **86**, 056303 (2012).